Astronomy & Astrophysics manuscript no. 12097
September 16, 2009

Na-O Anticorrelation and HB. VIII. Proton-capture elements and metallicities in 17 globular clusters from UVES spectra⋆,⋆⋆

Eugenio Carretta[1], Angela Bragaglia[1], Raffaele Gratton[2], and Sara Lucatello[2,3]

[1] INAF-Osservatorio Astronomico di Bologna, Via Ranzani 1, I-40127 Bologna, Italy
[2] INAF-Osservatorio Astronomico di Padova, Vicolo dell'Osservatorio 5, I-35122 Padova, Italy
[3] Excellence Cluster Universe, Technische Universität München, Boltzmannstr. 2, D-85748, Garching, Germany

Received 18 March 2009 / Accepted 31 May 2009

ABSTRACT

We present homogeneous abundance determinations for iron and some of the elements involved in the proton-capture reactions (O, Na, Mg, Al, and Si) for 202 red giants in 17 Galactic globular clusters (GCs) from the analysis of high-resolution UVES spectra obtained with the FLAMES facility at the ESO VLT2 telescope. Our programme clusters span almost the whole range of the metallicity distribution of GCs and were selected to sample the widest range of global parameters (horizontal-branch morphology, masses, concentration, etc). In this paper we focus on the discussion of the Na-O and Mg-Al anticorrelations and related issues. Our study finds clear Na and O star-to-star abundance variations, exceeding those expected from the error in the analysis, in all clusters. Variations in Al are present in all but a few GCs. Finally, a spread in abundances of Mg and Si are also present in a few clusters. Mg is slightly less overabundant and Si slightly more overabundant in the most Al-rich stars. The correlation between Si and Al abundances is a signature of production of ^{28}Si leaking from the Mg-Al cycle in a few clusters. The cross sections required for the proper reactions to take over in the cycle point to temperatures in excess of about 65 million K for the favoured site of production. We used a dilution model to infer the total range of Al abundances starting from the Na and Al abundances in the FLAMES-UVES spectra, and the Na abundance distributions found from analysis of the much larger set of stars for which FLAMES-GIRAFFE spectra were available. We found that the maximum amount of additional Al produced by first-generation polluters contributing to the composition of the second-generation stars in each cluster is closely correlated with the same combination of metallicity and cluster luminosity that reproduced the minimum O-abundances found from GIRAFFE spectra. We then suggest that the high temperatures required for the Mg-Al cycle are only reached in the most massive and most metal-poor polluters.

Key words. Stars: abundances – Stars: atmospheres – Stars: Population II – Galaxy: globular clusters – Galaxy: globular clusters: individual: NGC 104 (47 Tuc), NGC 288, NGC 1904 (M 79), NGC 2808, NGC 3201, NGC 4590 (M 68), NGC 5904 (M 5), NGC 6121 (M 4), NGC 6171 (M 107), NGC 6218 (M 12), NGC 6254 (M 10), NGC 6388, NGC 6397, NGC 6441, NGC 6752, NGC 6809 (M 55), NGC 6838 (M 71), NGC 7078 (M 15), NGC 7099 (M 30)

1. Introduction

A growing body of evidence indicates that globular clusters (GCs) are not actual examples of simple stellar populations: when examined in detail, their stars are not coeval, nor do they share the same initial chemistry (see the exhaustive reviews by Kraft 1994 and, more recently, by Gratton, Sneden, Carretta 2004 on this subject). The star formation in GCs included a second generation of stars born from the ejecta of the most massive among the stars of the primeval generation. The first phases of evolution of GCs were likely complex, including a variety of dramatic and energetic phenomena like supernova explosions and high and low velocity winds from both blue and red massive stars, possibly combining in giant expanding bubbles of gas and shock fronts, which may have triggered further star formation. Even more complex might have been the environment for these events, possibly in the cores of giant clouds or even, in the case of the most massive clusters, of dwarf galaxies (Bekki 2006).

Most of these events left behind a trace, represented by the chemical composition of the stars, that can be followed through quite subtle spectral features, like the lines of O, Na, and another few key elements such as Al, Mg, and possibly Si. This allows us to quantitatively probe the existence of a second generation of stars in GCs.

The best known among these tracers is the star-to-star anticorrelation between the O and Na abundances, which has been

Send offprint requests to: E. Carretta, eugenio.carretta@oabo.inaf.it

⋆ Based on observations collected at ESO telescopes under programmes 072.D-507 and 073.D-0211

⋆⋆ Tables 1, 3, 4, 6, 8, and 9 are only available in electronic form at the CDS via anonymous ftp to `cdsarc.u-strasbg.fr` (130.79.128.5) or via `http://cdsweb.u-strasbg.fr/cgi-bin/qcat?J/A+A/???/???`

found in all GCs surveyed so far, at variance with field stars (see e.g. Gratton et al. 2000). This is the sign of (originally unexpected) material processed through the complete CNO and the Ne-Na cycles of proton capture reactions in -possibly- the majority of GC stars. The key study of non-evolved stars in GCs by Gratton et al. (2001) unambiguously showed that the processed material must originate in an earlier generation of stars (see also Cohen et al. 2002). Self-pollution models are not yet able to convincingly explain all observed features. Candidate first-generation polluters are thermally pulsing, intermediate-mass AGB stars undergoing hot bottom burning (see Ventura et al. 2001), or massive, rotating stars (see Decressin et al. 2007). Addition of new observational data is crucial to better constraining these models.

In addition to the CNO and Ne-Na cycle, there is evidence that the Mg-Al cycle is also active in GC polluters. The Mg-Al cycle provides information that is complementary to those provided by the Ne-Na cycle, mainly for two reasons: (*i*) it requires much higher temperatures (some 70 MK to be compared with 25 MK, see Charbonnel & Prantzos 2006), meaning that different polluters are possibly involved; (*ii*) while the Ne-Na cycle essentially saturates in most polluters, thus providing similar maximum Na abundances in most GCs, with only small (though detectable, see below) variations, no case of complete transformation of Mg into Al has been observed. The case of the Mg-Al is clearly more complex, because many nuclei are involved (the various Mg isotopes; see e.g. Yong et al. 2003), with possibly even some production of Si (see e.g. Yong et al. 2005). Hence, while an overall correlation between Na and Al might be expected (because they should share dilution effects like those considered by Prantzos & Charbonnel 2006), details of this correlation are not obvious and can provide crucial information on the nature of the polluters.

In addition to modifications in the distribution of products from H-burning at high temperature, GCs could significantly differ from the field population if the proto-GCs were able to have some independent chemical evolution, retaining at least part of the metal-enriched ejecta of core-collapse SNe (e.g, Cayrel 1986; Parmentier & Gilmore 2001). Observationally, we might expect that GCs have a higher [α/Fe][1] ratio than field stars of similar metal abundance, as well as possibly other peculiar abundance patterns (concerning e.g. primordial Al and Na abundances). These signatures are likely subtle and might have escaped detection in literature data, lacking in homogeneity.

In this series of paper we are presenting a very extensive new set of data on abundances in several Galactic GCs, selected to span all the ranges of different physical parameters (metallicity, concentration, density, HB morphology, mass, etc.), obtained exploiting the ESO multi-fibre FLAMES facility. This survey (see Carretta et al. 2006a, hereafter Paper I) aims to provide significant constraints and answers to fundamental questions such as: *(i)* Were GC stars really born in a single "instantaneous" burst? *(ii)* Did GCs self-enrich? *(iii)* How do abundance anomalies within each individual GC relate to the formation and early evolution of the GC itself and of each individual member?

Using FLAMES/GIRAFFE spectra of more than 2000 stars in 19 GCs we have singled out in a companion paper (Carretta et al. 2009, hereinafter Paper VII) second-generation stellar populations in many GCs. Using the Na-O anticorrelation as a diagnostic, we studied the enrichment history in GCs. The main results of that paper were that

i) the Na-O anticorrelation is present in all GCs and the second generation stars (that we separate into an intermediate and extreme I and E populations) dominate the first generation stars (that we called primordial P population);
ii) the E and P populations are more numerous among the most massive clusters;
iii) the shape of the Na-O anticorrelation changes regularly (from more extended and shallow to less extended and steep) as a function of cluster metallicity and luminosity (this last a likely proxy for the average polluter mass);
iv) the amount of Na produced in more luminous and metal-poor clusters is close to what is expected from simple transformation of all ^{22}Ne originally available in the polluters into ^{23}Na, while an extra-amount of ^{22}Ne (possibly due to primary production from triple-α burning) is required in less luminous and metal-rich clusters.

In this paper we present the analysis of the high-resolution UVES spectra that we collected simultaneously with the moderate resolution GIRAFFE spectra, a unique and precious opportunity provided by the FLAMES multiobject facility. While only seven fibres can be devoted to UVES in each pointing (more than an order of magnitude less than for GIRAFFE), UVES spectra have a higher resolution and ten times wider spectral coverage. For this reason they were crucial in several respects:

1) to measure accurate O and Na abundances for additional stars beside those with GIRAFFE spectra; this point turned out to be important in some cases (e.g. NGC 6397) where O abundances could be derived only for a handful of stars from lower resolution GIRAFFE observations (see Paper VII);
2) to provide accurate measurements of equivalent widths (*EW*s) from high-resolution spectra to build a reference system on which to check the *EW*s measured on lower resolution GIRAFFE spectra for each cluster;
3) to obtain abundances for the proton-capture element Al with no transition falling in the spectral range covered by the two GIRAFFE gratings used (HR11 and HR13);
4) to define a new metallicity scale based on accurate measurements in a large sample of clusters, homogeneously derived with modern sets of near infrared magnitudes (from 2MASS, Skrutskie et al. 2006), atmospheric parameters (from the calibration by Alonso et al. 1999), and atomic parameters (from the compilation by Gratton et al. 2003);
5) to test the idea by Cayrel (1986) that proto-GCs might have been able to sustain some independent chemical evolution, aside from modification in CNO elements, retaining at least

[1] We adopt the usual spectroscopic notation, *i.e*. [X]= $\log(X)_{star} - \log(X)_{\odot}$ for any abundance quantity X, and $\log \epsilon(X) = \log (N_X/N_H) + 12.0$ for absolute number density abundances.

Table 1. Log of the UVES observations (complete table available only in electronic form

GC	date	UT	Texp	airmass
NGC0104	2004-06-26	09:47:32.114	1600	1.497
	2004-07-07	09:09:12.509	1600	1.494
	2004-07-07	09:47:22.887	1600	1.478

part of the metal-enriched ejecta of core-collapse supernovae.

Previous papers of this project have focused on a few particular clusters, tuning our procedures for the analysis of huge samples of stars and for estimates of error sources, especially from GIRAFFE spectra. In the companion Paper VII we presented the Na-O anticorrelation derived for almost 2000 red giant branch (RGB) stars and provided a synoptic table with references to all the analyses. UVES spectra were only exploited up to now to measure the detailed chemical composition of two poorly studied, yet interesting bulge clusters (NGC 6441, Gratton et al. 2006, Paper III; and NGC 6388, Carretta et al. 2007b, Paper VI), for a total of 12 stars. In the present paper we present the analysis of the other 202 RGB star with UVES spectra that are *bona fide* members in the remaining 17 clusters of our sample. We focus our discussion on the additional information they can provide about the proton capture process (the first three items listed above), while an in depth analysis of the information concerning primordial abundances as well as star-to-star scatter in Fe abundances will be presented in future works. The most crucial additional data concern the Mg-Al cycle, which could not be observed on the GIRAFFE spectra for lack of Al lines. (We selected the two gratings including the O and Na spectral features most suited for abundance determination).

The outline of the paper is as follows. Criteria of target selection and observations are given in the next section; our procedure deriving the atmospheric parameters and the analysis are described in Sect. 3, whereas error estimates are briefly discussed in Sect. 4. In Sect. 5 we show the pattern of Na-O and Mg-Al anticorrelations in all clusters, while Sect. 6 is devoted to extending and tuning the simple dilution model set up in the companion Paper VII, with a comparison with predictions from models of massive stars (both in main sequence and in the AGB phase). Finally, results are summarised in Sect. 7.

2. Target selection and observations

Our observations were collected in Service Mode at the ESO VLT-UT2 telescope under programmes 072.D-0507 and 073.D-0211 using the high-resolution multifibre facility FLAMES (Pasquini et al. 2002). In Table 1 we list the log of observations for each cluster; date and time of beginning of the observations are UT, exposure times are in seconds. The reported airmass is the one at the start of each exposure. The UVES Red Arm fed by FLAMES fibres provides a wavelength coverage from 4800 to 6800 Å with a resolution of $R \simeq 40,000$.

Cluster selection- The first criterion adopted was to select clusters with a wide range of distribution of stars along the HB, since this project mainly focused on studying possible relations between the morphology of the HB and the chemical composition of different stellar generations in clusters. In our sample all HB morphologies are represented, from the stubby red type to clusters with only blue HBs and with very extended blue tails, passing through bimodal or red and blue HB morphologies. Second, since the metallicity is the well-known *first* parameter in shaping the HB morphology, we inserted GCs with metal abundances from [Fe/H]= -2.4 to about [Fe/H]= -0.4 in our sample, spanning almost the whole metallicity range of the Galactic GCs. Both small and massive clusters are included in our sample, and finally all the age classes defined by Zinn, Lee, and collaborators (see e.g. Mackey and van den Bergh 2005) are represented well in the sample (see also Carretta et al. 2009, Paper VII). In Table2 we provide some information for the sample analysed here. After the cluster alternate name we list the number of member stars observed, together with their average effective temperature and the mean S/N per pixel, estimated around 6200 Å.

Star selection- The target selection within a given cluster followed the same criteria already illustrated for the previous GCs. We chose stars free of any companion brighter than $V + 2$ mag within a 2.5 arcsec radius, or brighter than $V - 2$ mag within 10 arcsec, with V the target magnitude. Stars near the RGB ridge line were primarily selected, while stars close to the RGB tip were avoided to reduce problems related to model atmospheres. We used two fibre configurations to maximize the number of possible target observed with UVES dedicated fibres (up to a maximum of seven, plus one pointing to the sky) while observing the bulk of programme stars with the GIRAFFE instrument. The constraints due to mechanical limitations in the Oz-Poz fibre positioner for FLAMES, coupled with the clusters sizes on the sky, restricted observations to stars at some distance from the clusters centres. However, these circumstances did not increase the risk of including field interlopers much except for the disc cluster NGC 6171 (M 107), where we found that only five UVES fibres targeted cluster member stars. Relevant information for all individual target stars (cluster, star identification, coordinates, magnitudes, and heliocentric radial velocities) are given in Table 3 (on-line).

Photometry and astrometry- We used the available optical photometry, calibrated to the standard Johnson-Cousins system, for our target selection. The adopted photometric and astrometric data are discussed in Carretta et al. (2006, Paper I) for NGC 2808, in Carretta et al. (2007a, Paper II) for NGC 6752, in Carretta et al. (2007c, Paper IV) for NGC 6218 (M 12), and in Carretta et al. (2009, Paper VII) for the remaining clusters analysed here. The K magnitudes used for the determination of effective temperature and surface gravity (see next section) are from the 2MASS Point Source Catalogue (Skrutskie et al. 2006). Optical and near IR magnitudes are listed in Table 3.

Spectroscopic data preparation- We used the one-dimensional, wavelength-calibrated, reduced spectra from

Table 2. Information on the observed GCs

GC	other	Nr_{stars}	$< T_{eff} >$	$< S/N >$	RV	σ	RV_{Harris}
NGC 104	47 Tuc	11	4125	95	-19.86	7.26	-18.7
NGC 288		10	4465	101	-46.15	2.55	-46.6
NGC 1904	M 79	10	4520	69	204.82	2.02	206.0
NGC 2808		12	4423	97	104.09	8.01	93.6
NGC 3201		13	4441	83	494.57	3.85	494.0
NGC 4590	M 68	13	4668	86	-94.35	2.24	-94.3
NGC 5904	M 5	14	4438	70	53.78	5.91	52.6
NGC 6121	M 4	14	4329	91	71.95	4.07	70.4
NGC 6171	M 107	5	4427	40	-38.82	9.55	-33.6
NGC 6218	M 12	11	4385	80	-41.25	3.61	-42.2
NGC 6254	M 10	14	4531	88	74.57	4.39	75.8
NGC 6397		13	4798	79	22.75	7.10	18.9
NGC 6752		14	4363	100	-26.96	6.01	-27.9
NGC 6809	M 55	14	4440	77	174.83	4.33	174.8
NGC 6838	M 71	12	4064	92	-23.97	2.56	-22.8
NGC 7078	M 15	13	4668	84	-107.34	5.08	-107.0
NGC 7099	M 30	10	4600	84	-188.05	5.20	-181.9

Table 3. List and relevant information for the 202 target stars in 17 GCs. The complete table is available electronically only at CDS; we show here a few lines for guidance.

GC	ID	RA	Dec	B	V	I	K	RV(Hel)	rms
NGC 104	5270	0 24 16.877	-72 11 49.47	13.654	12.272	0.000	8.838	-10.25	0.01
NGC 104	12272	0 23 55.015	-72 08 23.67	13.732	12.433	0.000	9.122	-11.96	0.46
NGC 104	13795	0 25 13.285	-72 07 50.43	13.813	12.553	0.000	9.431	-28.88	0.01
NGC 104	14583	0 22 31.979	-72 06 48.99	14.118	12.878	0.000	9.831	-11.90	0.02
NGC 104	17657	0 25 04.269	-72 06 39.87	13.697	12.252	0.000	8.628	-24.12	0.31

the ESO UVES-FLAMES pipeline (uves/2.1.1 version) as prepared by the ESO service mode personnel. Radial velocities (RVs) were measured for each individual spectrum using many lines with the IRAF[2] package RVIDLINES. Using these RVs the spectra were shifted to zero RV and co-added for each star. The resulting heliocentric RVs and associated errors (typically a few hundred m s^{-1}) are indicated in Table 3 for individual member stars; average values for each programme cluster (with 1σ rms scatters) are listed in Table 2 with the values from the Harris (1996) updated catalogue, as a comparison. In almost all cases it was possible to disregard non member stars on the basis of the RVs. Only in NGC 6218 were two stars, considered probable members from their RVs, rejected on the basis of the resulting abundances as field interlopers (see also Paper IV). For the first two clusters analysed (NGC 6218 and NGC 6752), we used the full spectral coverage of the UVES red arm spectra, from about 4800 Å to about 6800 Å. Afterwards, we restricted the analysis to the range 5600-6800 Å in order (i) to have a complete overlap with the spectral range of the GIRAFFE HR11 and HR13 gratings for the intercomparison of the EWs, and (ii) to exploit a region in wavelength where the S/N was higher and the line crowding lower. For the three most metal-poor clusters (NGC 6397, NGC 7078, and NGC 7099) we had to use the entire wavelength range to increase the number of useful lines; however, line crowding was negligible even in the blue-yellow part of their spectra.

[2] IRAF is distributed by the National Optical Astronomical Observatory, which are operated by the Association of Universities for Research in Astronomy, under contract with the National Science Foundation

3. Atmospheric parameters and analysis

3.1. Atmospheric parameters

Temperatures and gravities were derived for all stars using the same procedure described in detail in the previous papers of the series (see Papers II to VII) to which we refer the reader. The only exception was NGC 2808 (Paper I). For this cluster, the first analysed, temperatures were obtained only from $V-K$ colours and the Alonso et al. (1999) calibration, without using the second step of deriving the final adopted temperatures from a $T_{\rm eff}$ versus magnitude relation. For self-consistency, we used here the same temperature derivation also for stars in NGC 2808 observed with UVES that, furthermore, were all observed with both instruments.Surface gravities were obtained from the position of stars in the colour-magnitude diagram.

Microturbulent velocities, v_t, were derived by eliminating trends in the relation between abundances from Fe neutral lines and expected line strength (see Magain 1984). Final metallicities were obtained by interpolating the model with the proper atmospheric parameters whose abundance matched the one derived from Fe I lines in the Kurucz (1993) grid of model atmospheres (with overshooting on).

Adopted atmospheric parameters, along with iron abundances derived from neutral and singly ionised lines, are listed

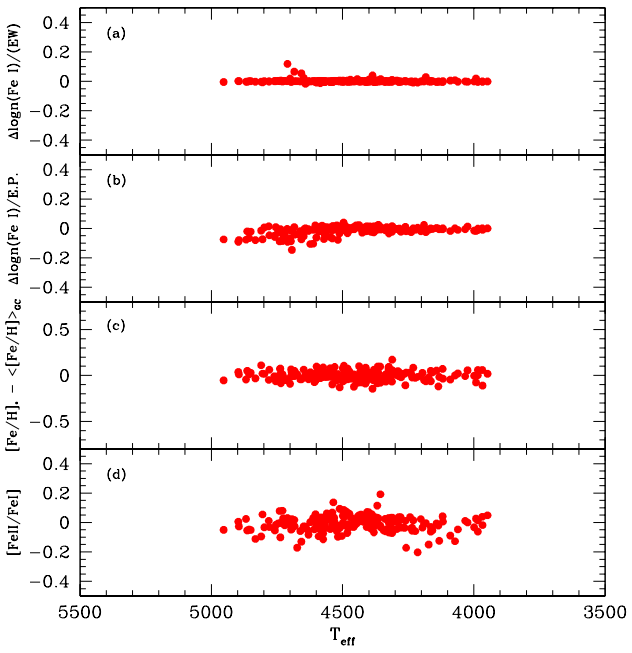

Fig. 1. A graphical summary for the analysis of iron abundances in the 202 red giant stars with UVES spectra in the 17 GCs analysed here. (*a*): slope of the relation between expected line strength and Fe I abundances used to derive the v_t values for each individual stars. (*b*) slope of the relation between Fe I abundances and excitation potential E.P. for each star. (*c*): the average [Fe/H] value for each cluster is subtracted from the metallicity of each star in the cluster, and the differences are shown. (*d*): differences in iron abundances from Fe I and Fe II lines. All quantities are plotted as a function of the effective temperature.

in Table 4 (completely available only in electronic form at CDS) for all the 202 stars with UVES spectra analysed in the 17 GCs of the present work.

3.2. Equivalent widths and iron abundances

The adopted line lists, atomic parameters, and reference solar abundances (from Gratton et al. 2003) are strictly homogeneous for all stars analysed in all clusters of the present programme. We stress that this is the remarkable strength of the project, aimed at obtaining an extensive database of stellar abundances derived in the most homogeneous way for a significant part of the galactic GC population.

Equivalent widths were measured with the same automatic procedure as we used in the analysis of GIRAFFE spectra (Papers I, II, VI, V, VII; see the detailed description in Bragaglia et al. 2001 for the definition of the local continuum around each line). Stars observed in each cluster with both instruments were used to register the *EW*s from GIRAFFE spectra to those measured here on the higher resolution UVES spectra (see also the discussion in Paper VII), using linear relations to correct the *EW*s.

After this correction onto the UVES system is applied, *EW*s from GIRAFFE spectra agree very well with those measured even in extremely high-resolution spectra with quite high S/N (see a lengthier discussion in Paper II, section 2.2).

Average abundances of iron derived from UVES spectra for the 17 programme clusters are summarised in Table 5, where we include also the 2 bulge clusters (NGC 6388 and NGC 6441) previously analysed in Papers III and VI. Beside the number of stars for each cluster, we list in this table the average value of [Fe/H] with two attached errors: the first is the statistical error and the second represents the systematic error related to the various assumptions we made in the analysis (see below, next section)[3] . The *rms* scatter about the mean is given in the next column of Table 5.

The average slope $\Delta\theta$ of the relation between abundances from Fe I lines and excitation potential and the average slope in the relation of the expected line strength versus Fe I (used to derive the microturbulent velocity) are given in the next two columns, each with its statistical error attached. Individual values of these slopes are plotted as a function of the adopted effective temperature in the first two panels of Fig. 1 which summarises our analysis of iron abundances in the 17 programme clusters. Panel (a) shows how well the microturbulent velocity is constrained by our using several tens of Fe I lines and the expected line strength: the average value is 0.002 ± 0.001 with $rms = 0.012$ from 202 stars, stable even when a $2.5\sigma-$clipping is applied. Panel (b) in Fig. 1 displays the slopes of the relation between abundances from neutral Fe I lines and excitation potential for each analysed star. There is a slight trend toward more negative value for lower metallicity stars, the average value for the 202 stars being -0.013 ± 0.002 with $rms = 0.029$, which implies that we derive temperatures from colours about 45 K higher than those we would derive from the iron excitation equilibrium. However, after excluding 32 outliers with a $2.5\sigma-$clipping, the average slope becomes only -0.004 ± 0.001 (with $rms = 0.013$), corresponding to an offset in temperature of only about 14 K.

To plot the metal abundance of single stars for all clusters, we subtracted the average metallicity of the parent cluster from each star. The results are plotted in panel (c) of Fig. 1 and show no trend whatsoever as a function of the temperature (on a range of $\sim$ 1000 K), the mean difference being 0.000 ± 0.004 with $rms = 0.050$ dex, after 3 outliers were eliminated by a $2.5\sigma-$clipping.

Finally, the last two columns of Table 5 list the average [Fe II/Fe I] ratio for each cluster and its *rms* scatter of the mean. Individual values are plotted in the last panel (d) of Fig. 1 and the average value from 191 stars left after the usual clipping of outliers is -0.004 ± 0.003 ($rms = 0.042$ dex). This difference is obviously negligible and it indicates that the iron ionisation equilibrium is perfectly matched by our present abundance analysis. In turn, since surface gravities are derived from the position in the colour-magnitude diagram, this evidence supports the assumptions we made in the analysis very well,

[3] As discussed in Paper IV these systematic errors only include uncertainties in the average cluster abundances. Limitations due to e.g. the grid of model atmospheres used or to the reference solar abundances, which apply to all clusters, are not included.

Table 4. Atmospheric parameters and iron abundances. The complete table is available only in electronic form at CDS.

GC	Star	$T_{\rm eff}$ (K)	log g (dex)	[A/H] (dex)	v_t (km s^{-1})	nr	[Fe/H]I (dex)	*rms*	nr	[Fe/H]II (dex)	*rms*
NGC 104	5270	3999	1.01	-0.77	1.48	88	-0.772	0.101	8	-0.804	0.130
NGC 104	12272	4061	1.14	-0.75	1.64	90	-0.747	0.102	6	-0.794	0.134
NGC 104	13795	4183	1.30	-0.83	1.49	72	-0.832	0.093	7	-0.836	0.089
NGC 104	14583	4231	1.47	-0.68	1.54	72	-0.684	0.070	7	-0.669	0.098
NGC 104	17657	3992	0.99	-0.84	1.56	79	-0.844	0.088	6	-0.818	0.143

Table 5. Iron abundances from UVES spectra.

GC	nr stars	[Fe/H]I ±stat.err.±syst. (dex)	*rms*	$<\Delta\theta>$ ±stat.err	$<\Delta$(FeI)$/EW>$ ±stat.err	<[FeII/FeI]>	*rms*
NGC 104	11	−0.768±0.016±0.031	0.054	−0.008±0.003	+0.003±0.004	−0.031	0.073
NGC 288	10	−1.305±0.017±0.071	0.054	−0.009±0.002	−0.001±0.001	−0.044	0.047
NGC 1904	10	−1.579±0.011±0.069	0.033	+0.004±0.002	+0.000±0.000	+0.031	0.026
NGC 2808	12	−1.151±0.022±0.050	0.075	−0.007±0.002	−0.002±0.001	−0.015	0.031
NGC 3201	13	−1.512±0.018±0.075	0.065	+0.016±0.003	+0.002±0.001	+0.049	0.064
NGC 4590	13	−2.265±0.013±0.070	0.047	−0.069±0.010	+0.022±0.010	−0.001	0.073
NGC 5904	14	−1.340±0.014±0.064	0.052	+0.001±0.003	+0.001±0.002	−0.003	0.034
NGC 6121	14	−1.168±0.012±0.054	0.046	+0.001±0.003	+0.000±0.000	−0.002	0.025
NGC 6171	5	−1.033±0.029±0.038	0.064	+0.009±0.006	+0.000±0.001	−0.037	0.031
NGC 6218	11	−1.330±0.013±0.066	0.042	−0.012±0.004	+0.001±0.001	−0.037	0.017
NGC 6254	14	−1.575±0.016±0.076	0.059	−0.017±0.004	+0.001±0.001	−0.021	0.071
NGC 6388	7	−0.441±0.014±0.025	0.038	−0.018±0.003	−0.000±0.003	+0.072	0.103
NGC 6397	13	−1.988±0.012±0.061	0.044	−0.036±0.008	+0.000±0.001	−0.039	0.019
NGC 6441	5	−0.430±0.026±0.050	0.058	−0.028±0.013	−0.002±0.001	+0.006	0.197
NGC 6752	14	−1.555±0.014±0.074	0.051	−0.005±0.002	+0.002±0.001	+0.034	0.017
NGC 6809	14	−1.934±0.017±0.074	0.063	+0.002±0.003	+0.005±0.003	+0.011	0.036
NGC 6838	12	−0.832±0.018±0.051	0.061	−0.004±0.002	−0.002±0.000	−0.022	0.049
NGC 7078	13	−2.320±0.016±0.069	0.057	−0.042±0.010	−0.000±0.001	−0.034	0.053
NGC 7099	10	−2.344±0.015±0.069	0.049	−0.041±0.013	+0.000±0.000	+0.003	0.070

namely the temperature scale and the adopted distance moduli and reddening values.

A comparison between iron abundances as obtained from GIRAFFE (in Papers I, II, IV, V, and VII) and UVES spectra (Papers III, VI, and the present paper) is plotted in Fig. 2 for all 19 GCs in our sample. In the upper panel the comparison is done for neutral iron, while abundances from singly ionised species are used in the lower panel. All data points lie within 1σ *rms* on the line of equal abundance, convincingly showing how homogeneous are our final metallicities. We therefore consider that the samples of stars observed with both the GIRAFFE and UVES spectrographs can be safely merged, as done in Paper VII to increase statistics and study the properties of stars belonging to different stellar generations in GCs.

4. Errors in the atmospheric parameters

Our procedure to estimate errors is described in detail in previous papers so will not be repeated here. In the present analysis we followed all the steps given in the extensive Appendix A of the companion Paper VII. In the following we address only differences with respect to that error analysis.

Sensitivities of abundance ratios to atmospheric parameters- We have 173 stars with UVES spectra observed also with GIRAFFE. Since the temperature range is quite similar for the two samples, we adopted the sensitivities for the elements Fe I, Fe II, O, and Na from Paper VII. For the elements not studied in that work (i.e., Mg, Al, and Si), we obtained the new sensitivity values by repeating our abundance analysis for each star and changing only one atmospheric parameter each time. For every cluster the adopted sensitivity to each parameter is the average of what results from the individual stars. In doing so, we also checked that the slope abundance/parameters for iron were similar to those obtained from GIRAFFE spectra. Table 6 lists the abundance changes of Mg, Al, and Si to the indicated variations in atmospheric parameters for the 17 clusters analysed here.

Errors in atmospheric parameters- Both star-to-star (internal) and systematic errors associated to the adopted atmospheric parameters were derived as in Appendix A of Paper VII and are summarised in Table 7 for our 17 programme clusters.

The main differences (in particular w.r.t. the estimates from GIRAFFE spectra) are:

– In the case of NGC 2808 the adopted temperatures were not derived from the relation with the magnitude; as a result,

Table 6. Sensitivities of abundance ratios to errors in the atmospheric parameters. The complete table is only available in electronic form.

	ΔT_{eff} = 50 K			Δv_t = +0.1 km/s		
cluster	Δ[Mg/Fe]	Δ[Al/Fe]	Δ[Si/Fe]	Δ[Mg/Fe]	Δ[Al/Fe]	Δ[Si/Fe]
NGC 104	−0.001	+0.032	−0.049	+0.019	+0.022	+0.026
NGC 288	−0.018	−0.012	−0.052	+0.015	+0.023	+0.019
	$\Delta \log g$ = +0.2 dex			Δ [A/H] = +0.1 dex		
cluster	Δ[Mg/Fe]	Δ[Al/Fe]	Δ[Si/Fe]	Δ[Mg/Fe]	Δ[Al/Fe]	Δ[Si/Fe]
NGC 104	−0.022	−0.038	+0.018	−0.007	−0.022	+0.005
NGC 288	−0.009	−0.012	+0.025	−0.004	−0.004	+0.012

Table 7. Star-to-star errors and cluster errors in atmospheric parameters and in the EWs from UVES

	star-to-star errors					cluster errors			
cluster	T_{eff} (K) (1)	log g dex (2)	[A/H] (dex) (3)	v_t (km/s) (4)	EW (dex) (5)	T_{eff} (K) (6)	log g dex (7)	[A/H] (dex) (8)	v_t (km/s) (9)
NGC 104	6	0.020	0.054	0.06	0.010	40	0.059	0.031	0.018
NGC 288	6	0.041	0.054	0.08	0.010	63	0.061	0.071	0.025
NGC 1904	5	0.041	0.033	0.06	0.011	57	0.060	0.069	0.019
NGC 2808	44	0.020	0.075	0.06	0.010	42	0.059	0.050	0.017
NGC 3201	4	0.041	0.065	0.05	0.011	62	0.061	0.075	0.014
NGC 4590	4	0.041	0.047	0.38	0.020	69	0.061	0.070	0.105
NGC 5904	12	0.041	0.052	0.05	0.012	54	0.060	0.064	0.013
NGC 6121	4	0.041	0.046	0.04	0.011	54	0.060	0.054	0.011
NGC 6171	2	0.041	0.064	0.07	0.014	26	0.057	0.038	0.031
NGC 6218	6	0.020	0.042	0.04	0.011	48	0.059	0.066	0.012
NGC 6254	4	0.041	0.059	0.09	0.012	67	0.061	0.076	0.024
NGC 6397	4	0.041	0.044	0.08	0.016	64	0.060	0.061	0.022
NGC 6752	5	0.041	0.051	0.03	0.011	58	0.060	0.074	0.008
NGC 6809	5	0.041	0.063	0.13	0.013	58	0.060	0.074	0.035
NGC 6838	5	0.041	0.061	0.06	0.012	45	0.059	0.051	0.017
NGC 7078	5	0.041	0.057	0.26	0.020	67	0.061	0.069	0.072
NGC 7099	5	0.041	0.049	0.12	0.018	71	0.061	0.069	0.038

the internal (star-to-star) error in effective temperature turns out to be about 8 times more than in the other clusters. This is good proof of the soundness of our approach.

- For the other clusters, errors in T_{eff} and gravity are as previously estimated in Paper VII
- Errors in metallicity do change because they are estimated from the *rms* scatter in [Fe/H] of all analysed stars.
- Errors in v_t are generally less than those from GIRAFFE spectra due to the much larger number of Fe I lines used to estimate the microturbulent velocity
- Errors from uncertainties in the measurement of *EW*s are lower, since they were obtained from the *rms* in Fe I divided by the square root of the typical number of measured lines, usually higher in UVES spectra, in particular in the case of iron.

Finally, in Table 8 we show the errors in the abundances of Fe (from neutral and singly ionised species), O, Na, Mg, Al, and Si as due to uncertainties in each atmospheric parameter and to errors in the *EW* measurement. The sums in quadrature of the three major (T_{eff}, v_t, *EW*) or of all error sources (last two columns in Table 8) represent the expected typical star-to-star error in each abundance ratio.

The observed scatter in Fe abundances will be compared to errors in a forthcoming paper. We only note here that as far as iron is concerned, this scatter is generally very small, so that the GCs can be still considered as monometallic aggregates. In turn, the implication is that products of supernovae nucleosynthesis must be very well mixed in the gas from which any protocluster started to form its stars. This is an inescapable constraint and requisite for any theoretical model of GCr formation.

Summarising, typical star-to-star errors for the 17 clusters in the present work are on average 0.088 dex in [O/Fe], 0.061 dex in [Na/Fe], 0.070 dex in [Mg/Fe], 0.078 dex in [Al/Fe], and 0.049 dex in [Si/Fe].

Table 8. Error in element ratios due to star-to-star errors in atmospheric parameters and in the EWs for UVES.The complete table is only available in electronic form.

	errors in abundances due to:						total star-to-star error		
	$T_{\rm eff}$	log g	[A/H]	v_t	<nr>	EW	$T_{\rm eff}$+v_t+EW	all	
[Fe/H]I	+0.004	+0.001	+0.003	−0.021	81	0.010	0.024	0.024	NGC 104
[Fe/H]II	−0.006	+0.004	+0.011	−0.009	7	0.035	0.037	0.038	
[O/Fe]	−0.003	+0.003	+0.009	+0.021	2	0.065	0.068	0.069	
[Na/Fe]	+0.001	−0.002	+0.000	+0.005	4	0.046	0.046	0.046	
[Mg/Fe]	+0.000	−0.002	−0.004	+0.011	3	0.053	0.054	0.054	
[Al/Fe]	+0.004	−0.004	−0.012	+0.013	2	0.065	0.066	0.068	
[Si/Fe]	−0.006	+0.002	+0.003	+0.016	8	0.033	0.037	0.037	

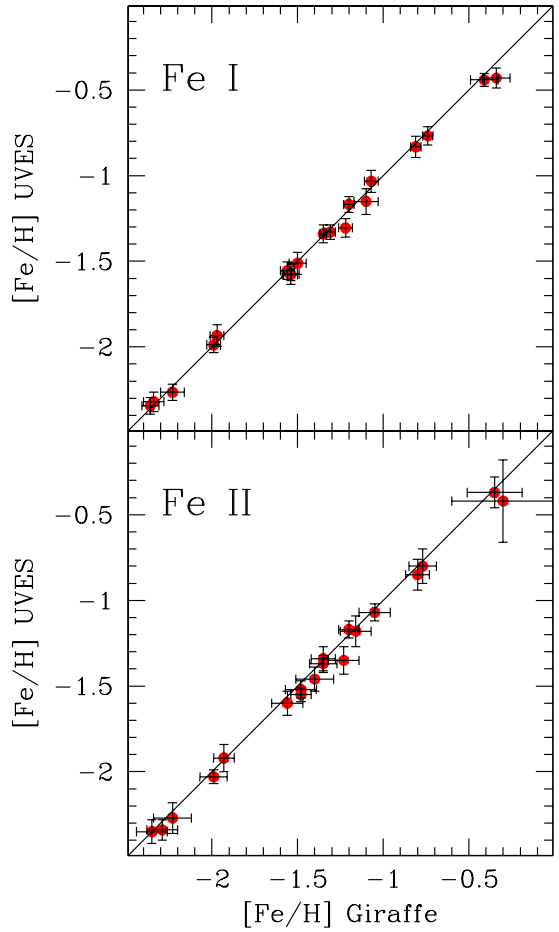

Fig. 2. Comparison for [Fe/H]ı ratios (upper panel) and for [Fe/H]ıı ratios (lower panel) obtained from GIRAFFE and UVES spectra in all the 19 programme clusters in our sample. Metal abundances from GIRAFFE are from Papers I,II,IV,V, and VII. Metallicities from UVES are from Papers III, VI ,and the present paper. Error bars are 1σ *rms* scatter and the solid line is the line of equality.

5. Results: proton-capture elements

In this section we discuss abundances for the light elements O, Na, Mg, Al, and Si participating in the chains of proton-capture reactions in H-burning at high temperature. These have been recognised for a long time as those responsible for generating the pattern of chemical composition typical of (and restricted only to) GC stars (see e.g. Denisenkov and Denisenkova 1989; Langer et al. 1993; and Gratton et al. 2004 for a recent review).

Abundances for these elements were obtained in the 202 RGB stars of the sample of 17 clusters analysed here from measured *EW*s.

Oxygen abundances are obtained from the forbidden [O ı] lines at 6300.3 and 6363.8 Å. We used a synthetic spectrum template (as described in Paper I) to clean each individual star spectra from telluric contamination by H_2O and O_2 lines in the region around the oxygen line at 6300.3 Å. The spectra were then shifted to zero RV and coadded. On the basis of previous experience, we consider as negligible the contributions to the measured oxygen *EW* due to the high excitation Ni ı line at 6300.34 Å and CO formation in our programme stars. Furthermore, as discussed in Papers III and VI, even when present these effects have opposite signs and compensate each other.

The Na abundances, derived from the doublets at 5682-88 Å and 6154-60 Å, were corrected for effects of departures from the LTE assumption using the prescriptions by Gratton et al. (1999). Mg abundances are typically based on two to three high excitation lines (Mg ı 5711.09, 6318.71 and 6319.24 Å) and Al abundances are all derived from the subordinate doublet at 6696-98 Å, the only one lying in the spectral region covered by UVES red arm spectra. The Si abundances are presented here because we found that in some clusters this element is partly involved, actually produced, in proton-capture reactions (see below)[4]. The Si abundances are from *EW*s of several transitions in the spectral range 5645-6145 Å; atomic parameters are from Gratton et al. (2003).

In Table 9 we list the abundances for the elements involved in proton-capture reactions at high temperature, derived for all stars with UVES spectra in the 17 programme clusters (the complete table is available only in electronic form at CDS). The table gives for each star the identification, the number of lines used, the abundance ratios, and the rms values; for O and Al, we distinguish between actual detections and upper limits.

We list in Table 10 the average abundances of O, Na, Mg, Al, and Si, together with the number of stars in each cluster and the 1σ rms scatter of the mean. In this table we include for completeness the ratios found for the two bulge clusters previously analysed in Papers III and VI. A simple comparison with

[4] The remaining α−elements for the combined large sample of stars with GIRAFFE and UVES spectra will be discussed in a forthcoming paper devoted to the scale of α− and Fe-group elements in GCs.

Table 9. Abundances of proton-capture elements in the 202 stars analysed. The complete table is available only electronically at CDS.

Star	n	[O/Fe] (dex)	rms	n	[Na/Fe] (dex)	rms	n	[Mg/Fe] (dex)	rms	n	[Al/Fe] (dex)	rms	n	[Si/Fe]	rms
NGC 104 05270	2	+0.122	0.059	4	+0.692	0.063	3	+0.550	0.133	2	+0.542	0.091	8	+0.429	0.065
NGC 104 12272	2	+0.270	0.025	4	+0.603	0.068	3	+0.573	0.065	2	+0.535	0.048	10	+0.429	0.100
NGC 104 13795	2	+0.359	0.028	4	+0.301	0.078	3	+0.502	0.140	2	+0.285	0.055	8	+0.384	0.086
NGC 104 14583	2	+0.344	0.035	4	+0.433	0.070	3	+0.545	0.055	2	+0.436	0.053	9	+0.417	0.055
NGC 104 17657	2	−0.068	0.136	4	+0.852	0.082	3	+0.496	0.161	2	+0.958	0.141	9	+0.364	0.161

Table 10. Mean abundance ratios in all the 19 GCs of our project.

Star	n	[O/Fe] (dex)	rms	n	[Na/Fe] (dex)	rms	n	[Mg/Fe] (dex)	rms	n	[Al/Fe] (dex)	rms	n	[Si/Fe] (dex)	rms
NGC 104	11	+0.25	0.15	11	+0.53	0.15	11	+0.52	0.03	11	+0.52	0.17	11	+0.40	0.02
NGC 288	10	+0.34	0.14	10	+0.29	0.28	10	+0.45	0.03	10	+0.40	0.09	10	+0.37	0.03
NGC 1904	9	+0.05	0.29	10	+0.42	0.29	10	+0.28	0.06	8	+0.64	0.41	10	+0.29	0.03
NGC 2808	12	+0.07	0.36	12	+0.20	0.24	12	+0.20	0.25	12	+0.40	0.49	12	+0.28	0.05
NGC 3201	13	+0.03	0.28	13	+0.16	0.31	13	+0.34	0.04	13	+0.14	0.38	13	+0.30	0.05
NGC 4590	13	+0.41	0.11	12	+0.33	0.19	13	+0.35	0.06	13	+0.74	0.18	13	+0.40	0.05
NGC 5904	14	+0.08	0.23	14	+0.25	0.24	14	+0.41	0.07	14	+0.27	0.29	14	+0.30	0.05
NGC 6121	14	+0.26	0.10	14	+0.40	0.15	14	+0.55	0.03	14	+0.60	0.05	14	+0.52	0.06
NGC 6171	5	+0.12	0.13	5	+0.49	0.15	5	+0.51	0.04	5	+0.39	0.07	5	+0.53	0.08
NGC 6218	11	+0.34	0.14	11	+0.30	0.27	11	+0.52	0.04	11	+0.20	0.18	11	+0.35	0.06
NGC 6254	14	+0.41	0.15	14	+0.17	0.19	14	+0.49	0.04	10	+0.41	0.37	14	+0.28	0.05
NGC 6388	7	−0.30	0.16	7	+0.59	0.16	7	+0.21	0.07	7	+0.69	0.24	7	+0.32	0.10
NGC 6397	13	+0.29	0.09	13	+0.18	0.19	13	+0.46	0.04				13	+0.34	0.05
NGC 6441	5	+0.12	0.20	5	+0.55	0.15	5	+0.34	0.09	5	+0.30	0.15	5	+0.33	0.11
NGC 6752	14	+0.16	0.28	14	+0.33	0.27	14	+0.50	0.05	14	+0.41	0.33	14	+0.38	0.05
NGC 6809	14	+0.16	0.11	14	+0.38	0.23	14	+0.47	0.10	14	+0.49	0.32	14	+0.38	0.06
NGC 6838	12	+0.31	0.13	12	+0.45	0.16	12	+0.49	0.04	12	+0.50	0.15	12	+0.38	0.06
NGC 7078	13	+0.34	0.19	13	+0.20	0.25	13	+0.45	0.19	13	+0.57	0.26	10	+0.43	0.10
NGC 7099	10	+0.46	0.20	10	+0.35	0.25	10	+0.51	0.04	10	+0.77	0.32	9	+0.34	0.07

star-to-star errors of Table 8 shows that the observed spreads in these element ratios clearly exceed those expected from uncertainties in the analysis, apart from the [Mg/Fe] and the [Si/Fe] ratios in some clusters.

This is immediately evident also from Fig. 3 (left panels), where for each cluster (including NGC 6388 and NGC 6441) the average ratios of the light elements [O/Fe], [Na/Fe], [Mg/Fe], [Al/Fe], and [Si/Fe] involved in the proton-capture reactions are superimposed on the same ratios for a large number of field stars spanning the same range in metallicity. Element ratios from field stars are from literature studies, mainly from the collection by Venn et al. (2004), and from abundance analyses not used by the Venn et al. compilation: Gratton et al. (2003), Fulbright et al. (2007), Reddy et al. (2003), Fulbright (2000), Johnson (2002), Jonsell et al. (2005), Gehren et al. (2006). The rms scatters associated in each study with abundances of field stars are typically less than a few hundredths of a dex, much smaller than those derived for the average abundances found in GCs for these elements.

From Table 10 and Fig. 3, it is possible to appreciate how cluster stars differ from their analogues in the galactic fields (irrespective of their belonging to the halo, disc, and bulge components). At every metallicity, the oxygen abundances are depleted on average and those of Na and Al are enhanced in GCs, with respect to the same ratios in field stars. The abundances of all these elements show large star-to-star variations that are not an effect of the analysis, but reflect a true change in chemical composition in a large fraction of stars (see also Paper VII). Differences between GCs and field populations are much less for Mg and Si, which also show much less spread. The smaller scatter for Mg and Si with respect to Al is in part an effect of their much larger primordial abundance; however, it also signals that only a fraction of the original Mg is transformed into Al and Si in the case of the Mg-Al cycle, at variance with the case of the Ne-Na cycle, where almost all ^{22}Ne is transformed into ^{23}Na. In turn, this is partly because of the higher temperature required for the reactions to occur in the two cycles (25 MK and 70 MK, respectively), and of complexity of the Mg-Al cycle itself (some of the original ^{24}Mg is transformed into ^{25}Mg and ^{26}Mg, rather than in ^{27}Al: see Yong et al. 2003). We come back to this point in next section.

On the other hand, if we consider the envelopes of the abundance distributions (upper for O and Mg; lower for Na, Al, and Si), we find good agreement between the abundances for the GCs and those for the field stars. This suggests that the abundances of the primordial population in GCs are close to those of the field stars -see also the right panels of Fig. 3, where the entire range of abundances in each cluster is shown. On the

whole, these are not new results (see e.g. Gratton et al. 2000 for a discussion of abundance variations in light elements in field stars as opposed to cluster stars), but in our study this comparison is based for the first time on a sample of cluster stars comparable in size with the samples of field stars. There are, however, subtler points that should be discussed, such as the large spread of the minimum values of [Al/Fe] ratios in the various clusters. We will re-examine this point in more detail in a forthcoming paper.

5.1. The Na-O anticorrelation

The present UVES spectra clearly reveal the classical anticorrelations between proton-capture elements, in spite of the limited number of UVES fibres available in each pointing that hampers a statistically meaningful study like the one on GIRAFFE data. In Fig. 4 we show the Na-O anticorrelations we obtain using only UVES observations for the 19 clusters observed within our programme (data from this paper, complemented by those for NGC 6441 from Paper III and NGC 6388 from Paper VI). Expected star-to-star error bars are plotted in each panel. Although limited in number in each cluster, these additional data are very useful in some cases: as explained in the companion Paper VII, the higher resolution and quality of UVES spectra are crucial where only a few upper limits in O abundances were extracted from a total of more than a hundred stars observed with GIRAFFE spectra, as happened for NGC 6397. In fact, the extreme homogeneity of our whole procedure allows the two sample of stars with UVES and GIRAFFE spectra to be safely merged, with gain in statistics. In Paper VII, whenever possible we replaced/complemented O and Na abundances obtained from GIRAFFE spectra with those from the UVES ones when studying the different stellar populations in GCs.

The global Na-O anticorrelation from UVES spectra for all programme clusters is plotted in the left panel of Fig. 5. Average error bars are also shown in this panel. The stars are colour-coded according to arbitrarily defined metallicity bins: stars of metal-rich clusters (-1.1 <[Fe/H] < -0.4 dex), giants of clusters of intermediate metallicity (-1.8 <[Fe/H] < -1.1 dex), and finally stars in the most metal-poor clusters (-2.4 <[Fe/H] < -1.8 dex). In the Na-O plane we can see that metal-rich clusters seem to start at the same average high oxygen values of the other GCs, but from a higher Na value, at the O-rich, Na-poor extreme of the anticorrelation. However, this is not surprising, because it is assessed that the plateau of minimum Na established by supernovae nucleosynthesis is a function of metallicity. It is higher for [Fe/H]> -1 dex, as is also evident from the literature data of field stars shown in Fig. 3. The largest extension of the Na-O anticorrelation seems to be reached in intermediate-metallicity clusters. Unpolluted stars (likely first-generation stars) in the most metal-poor clusters populate the same locus of unpolluted stars of GCs with moderate metal abundances; however, when the cluster metallicity is very low, the stars do not seem to show very large O-depletion. From this sample alone, it is not clear whether (and how much) this result might be affected by the difficulty of observing weak O lines in metal-poor, rather warm giants.

From the left panel of Fig. 5 we can see that the low-O ([O/Fe] $\lesssim -0.4$ dex) tail of the anticorrelation almost entirely come from stars measured in two clusters, NGC 2808 (three stars) and NGC 3201 (two stars)[5]. Actually, all *EW*s measured in these stars are upper limits and, from the quality of the spectra, we cannot determine at the moment what is the real O abundance. We note, however, that these three stars in NGC 2808 also have a subsolar [Mg/Fe] ratio (they actually define the low-Mg tail in the Mg-Al anticorrelation shown in the middle panel of Fig. 5), hence they are all good candidates for having chemical compositions severely altered by nuclear reactions involving all the proton-capture chains. In contrast, the other O-poor stars in this region from NGC 1904, NGC 3201, and NGC 5904 do not show any strong depletion of Mg, falling not much below the average value of the respective clusters. Finally, the last two stars in the O-poor tail belong to the metal-rich and quite massive cluster NGC 6388 (see Paper VI); also for these stars, the Mg abundances are not exceptionally low, since very close to the cluster average.

5.2. The Mg-Al cycle

Let us start by considering the abundances of the three elements involved in the Mg-Al cycle for which we have data (Mg, Al, and Si). We might expect some degree of anticorrelation between Mg and Al, and possibly even between Mg and Si, if the burning temperature is high enough. The central and right panels of Fig. 5 show the global anti-correlations that we derive from our sample of giants with UVES spectra. There is a considerable scatter in these plots. The Mg-Al run presents the same features already found by previous studies (see e.g. Cohen and Melendez 2005; Sneden et al. 2004). The star-to-star variations in Mg abundances are limited to a range of about 0.5 dex, in most cases much less, apart from very few exceptions; we stress that all the [Mg/Fe] values $\lesssim 0.2$ dex were checked by eye inspection of the spectral tracings. In the case of Mg and Si, there is no obvious anti-correlation: rather, there is a global positive correlation.

However, these global trends are only marginally instructive. In fact, there are large differences between individual clusters. Separate plots for each cluster provide much more insight. Such plots are shown in Figs. 6 and 7 for the Mg-Al and the Mg-Si relations, respectively. (In Fig. 6 NGC 6397 is excluded, since we did not measure Al in its stars.) An inspection of these figures reveals a few clear facts:

– The maximum Mg and minimum Al and Si abundances, which should be indicative of the composition of the primordial population (see next section) may be significantly different in different clusters. Although we observed only a limited number of stars in each cluster, and in many cases we were only able to derive upper limits to the Al abundances, there is little doubt that the minimum Al abundance may vary by almost an order of magnitude from cluster to cluster. In the next section we examine this issue in more

[5] The other two stars below [O/Fe]= -0.4 dex are from NGC 5904 and NGC 1904, respectively

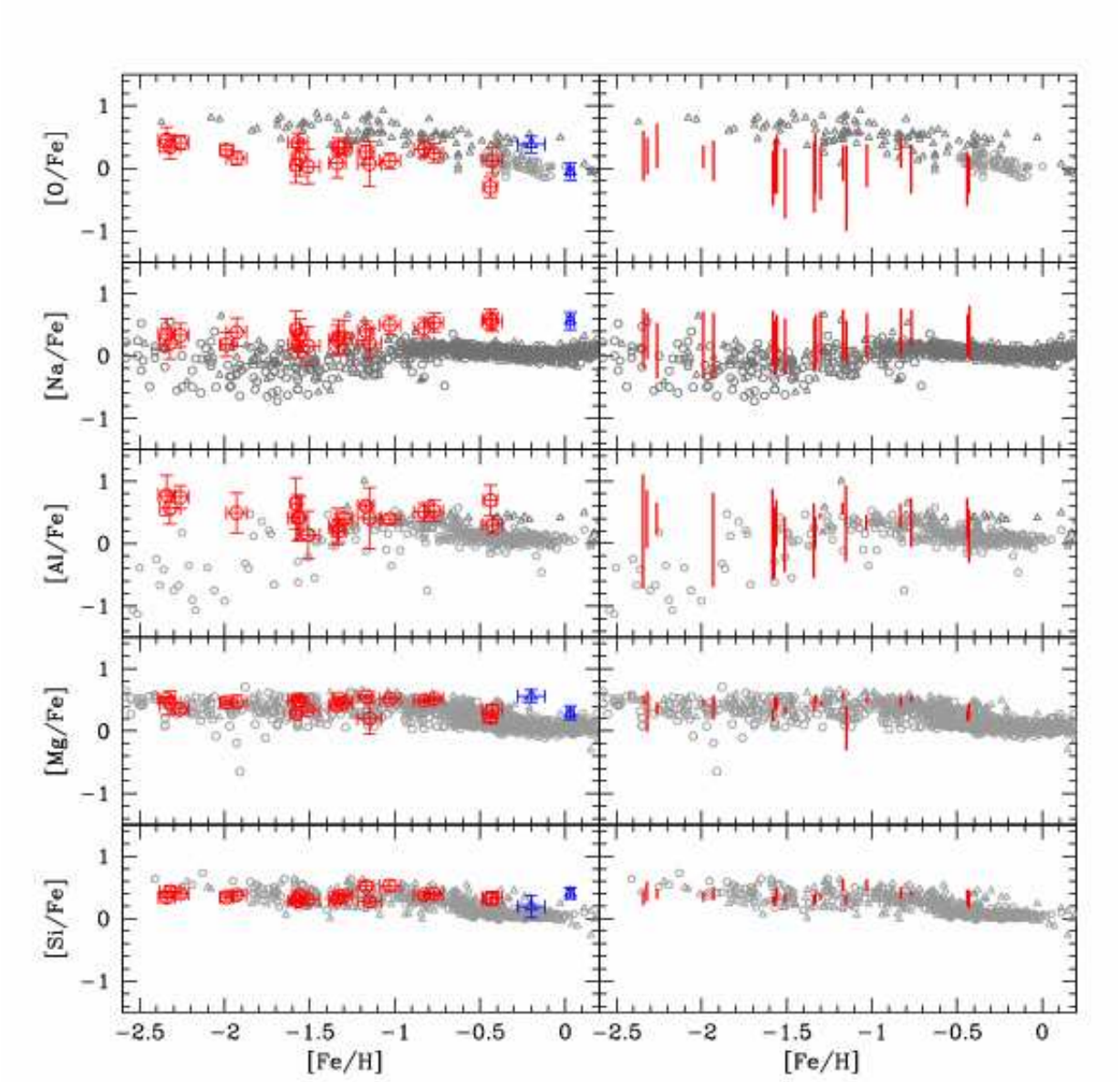

Fig. 3. Left panels: average ratios of O, Na, Al, Mg, and Si found in all 19 clusters of our project (large open circles), as a function of the metallicity, compared to the same ratios in field stars. We added the two bulge clusters NGC 6528 and NGC 6553, indicated by (blue) open triangles, also analysed by our group (Cohen et al. 1999; Carretta et al. 2001), as an extension to higher metallicities. From top to bottom: [O/Fe] average ratios superimposed on values from field stars from Gratton et al. (2003; empty squares), Fulbright et al. (2007; open triangles), and Reddy et al. (2003; open pentagons); average [Na/Fe] ratios for our clusters with ratios for field stars from Gratton et al. (2003), Fulbright et al. (2007), and the compilation by Venn et al. (2004; open circles); [Al/Fe] ratios are compared to values for field stars from Fulbright et al. (2007; open triangles), Fulbright (2000), Johnson (2002), Reddy et al. (2003), Jonsell et al. (2005) and Gehren et al. (2006): the last five studies are indicated by empty pentagons, collectively; finally, in the bottom panel average [Mg/Fe] ratios are compared to values for field stars from Gratton et al. (2003), Fulbright et al. (2007), and Venn et al. (2004), plotted as empty squares, triangles and circles, respectively. Error bars for the cluster averages are 1σ rms scatters of the mean. Right panels: we show the excursions for O, Na, Al, Mg, and Si in the 19 GCs of our sample, also superimposed on the same field stars.

detail, and try to obtain a better estimate of the minimum Al abundance for each cluster. On the other hand, maximum Mg and minimum Si abundances also change from cluster to cluster. Some cases are obvious, like the pair of clusters M 5 (NGC 5904) and M 4 (NGC 6121), for which such a difference has already been found in previous analyses (Carney 1996; Ivans et al. 1999, 2001). There is a good correlation between maximum Mg and minimum Si abundances derived from Figure 7. These values are displayed in Fig. 8, and both are well correlated with the maximum

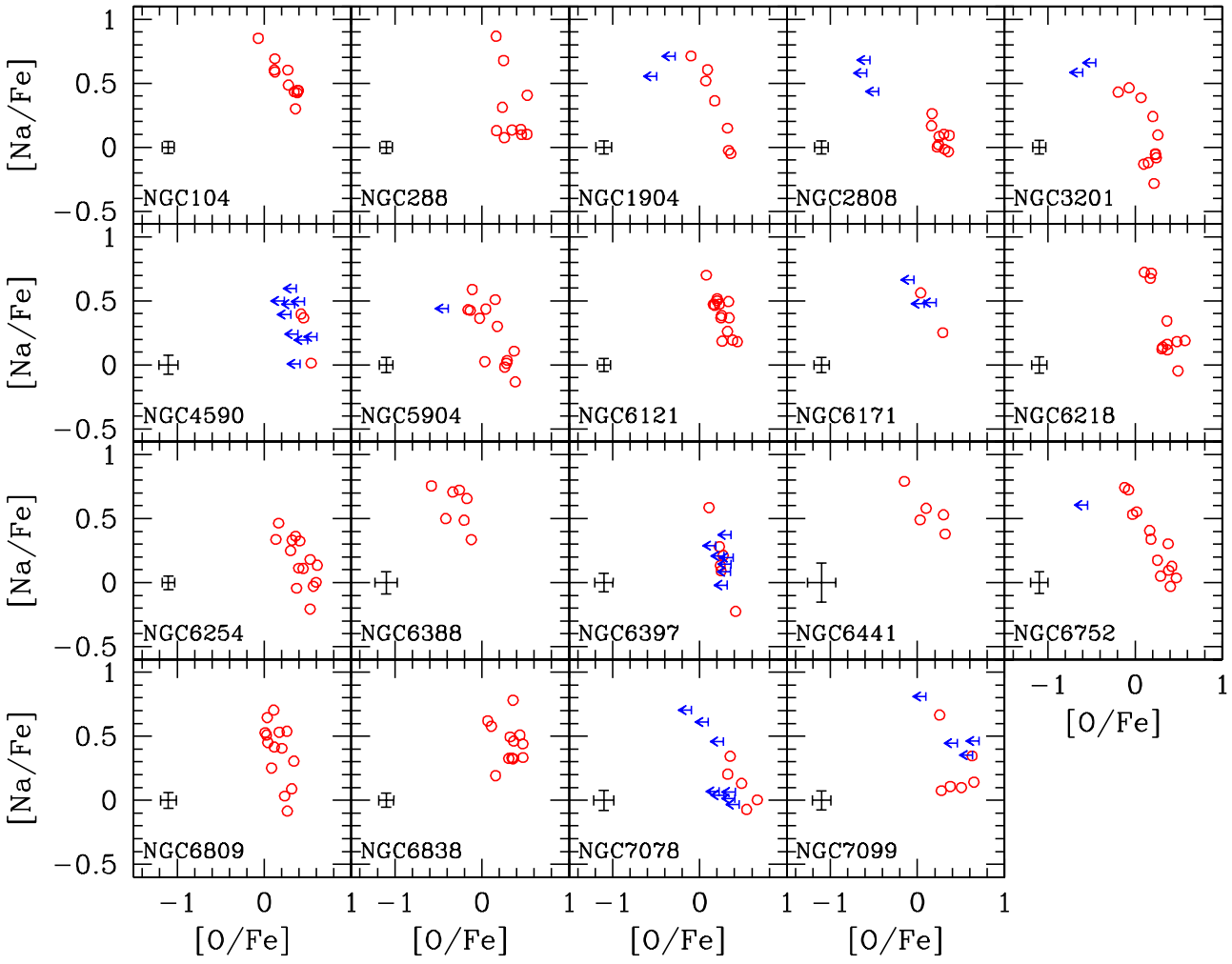

Fig. 4. The Na-O anticorrelation from UVES spectra observed in all the 19 GCs of our project (including NGC 6388 from Paper VI and NGC 6441 from Paper III). Star-to-star error bars (see Sect.4) are indicated in each panel. Upper limits in O abundances are shown as arrows, detections are indicated as open circles.

O abundance observed in each cluster. These fine correlations can be well explained by different primordial overabundances of the $\alpha-$elements in the various clusters. In a separate paper we will study the correlation existing between the overabundance of $\alpha-$elements and other cluster parameters. Here, we simply note that it justifies the global correlation of Mg and Si abundances.

– In a few clusters, none of these elements show significant variations. Such clusters are generally small and not very metal-poor. Typical cases are NGC 6121 (M 4), NGC 6171 (M 107), and NGC 288. We notice that all stars in these clusters have rather large Al abundances: this finding will be expanded upon in a future paper.
– In the remaining clusters, Al abundances show broad spreads. Clearly, these variations cannot be explained by observational errors (see Table 8). Interestingly enough, these are also approximately the same ranges of abundance variations as seen in unevolved cluster stars (Gratton et al. 2001), pointing to the same origin for the mechanism establishing the observed chemical pattern. Stars very rich in Al (with [Al/Fe]$\geq$ 0.8) show Mg depletion. This is not surprising, because Al is about an order of magnitude less abundant than Mg in the Sun and even more in the primordial stars in GCs. Hence, when a significant fraction of the original Mg is transformed into Al (so that the Mg depletion is detectable), Al production is comparatively huge. These Al-very rich and Mg-depleted stars are present in clusters that are massive (like NGC 2808, NGC 6388, NGC 6441), quite metal-poor (like NGC 6752), or both (like NGC 7078=M 15: note that, in this last case, we only have an upper limit to the Al abundance for the Mg-poor star). Hence, at variance with the Na-O anticorrelation, which is present in all GCs, the Mg-Al anticorrelation is present or particularly prominent only in massive and/or metal-poor GCs.
– The most extreme (low) Mg abundances have been detected in three NGC 2808 stars. Even these are actual detections, not upper limits. We remind the reader that this is one of the only two clusters showing a conspicuous component of second-generation stars with extreme composition (see

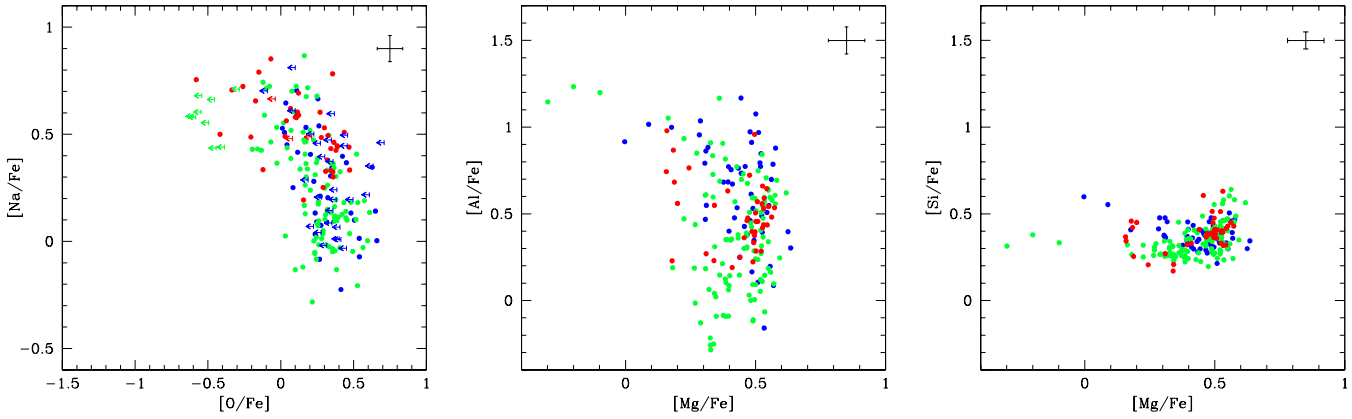

Fig. 5. Left panel: [Na/Fe] ratios as a function of [O/Fe] ratios in the 214 red giants with UVES spectra from the 19 clusters analysed (including NGC 6441 and NGC 6388). Stars are colour-coded according to cluster metallicity: in red stars of metal-rich clusters (-1.1 <[Fe/H] < -0.4 dex), in green giants of clusters of intermediate metallicity (-1.8 <[Fe/H] < -1.1 dex) and blue colours for stars in the most metal-poor clusters (-2.4 <[Fe/H] < -1.8 dex). Arrows indicate upper limits in O abundances. Central panel: the same, and with the same colour-coding. for the [Mg/Fe] ratios as a function of [Al/Fe] ratios. Right panel: the same, but for [Mg/Fe] and [Si/Fe].

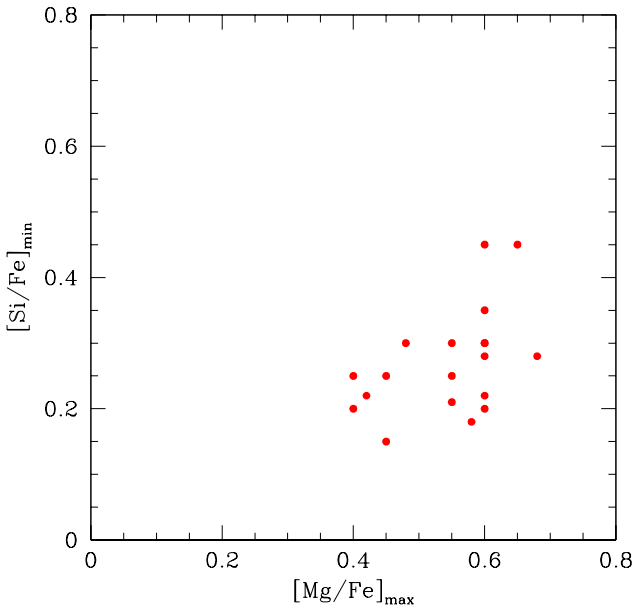

Fig. 8. $[Mg/Fe]_{max}$ versus $[Si/Fe]_{min}$ for the 19 GCs.

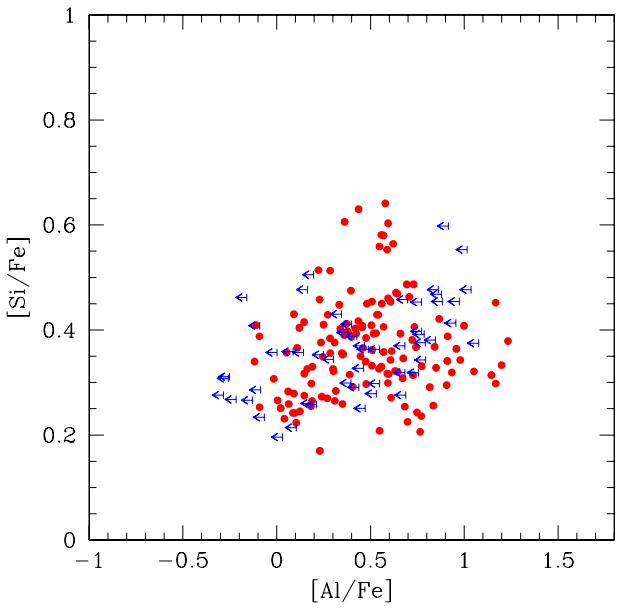

Fig. 9. Abundance ratio [Si/Fe] as a function of [Al/Fe] for stars with UVES spectra in all clusters of this project.

Paper VII), together with NGC 6205 (M 13; Sneden et al. 2004; Cohen and Melendez 2005). Furthermore, it is the *only* cluster where multiple main sequences of quite different He content (Piotto et al. 2007) have been identified so far (beside the peculiar case of ω Cen, with its multi-peaked metallicity distribution, see Piotto et al. 2005).

We further found that stars with extreme Al overabundance also show Si enhancement with respect to the remaining stars in the same cluster. Again, this effect is limited to massive or metal-poor GCs. We are aware of only one previous detection of the Al-Si correlation in a GC (NGC 6752: Yong et al. 2005). We now find that the effect is common among GCs, as illustrated by Fig. 9, where we show the correlation resulting by combining all stars. We found that the global slope (0.07 ± 0.02 from 192 stars) is highly statistically significant. Quantification of the amount of Si variation as a function of Al variation in each individual cluster is hampered by upper limits in Al abundances (see Fig.6). However,as Mg and Al are anticorrelated with each other, we can study the expected anticorre-

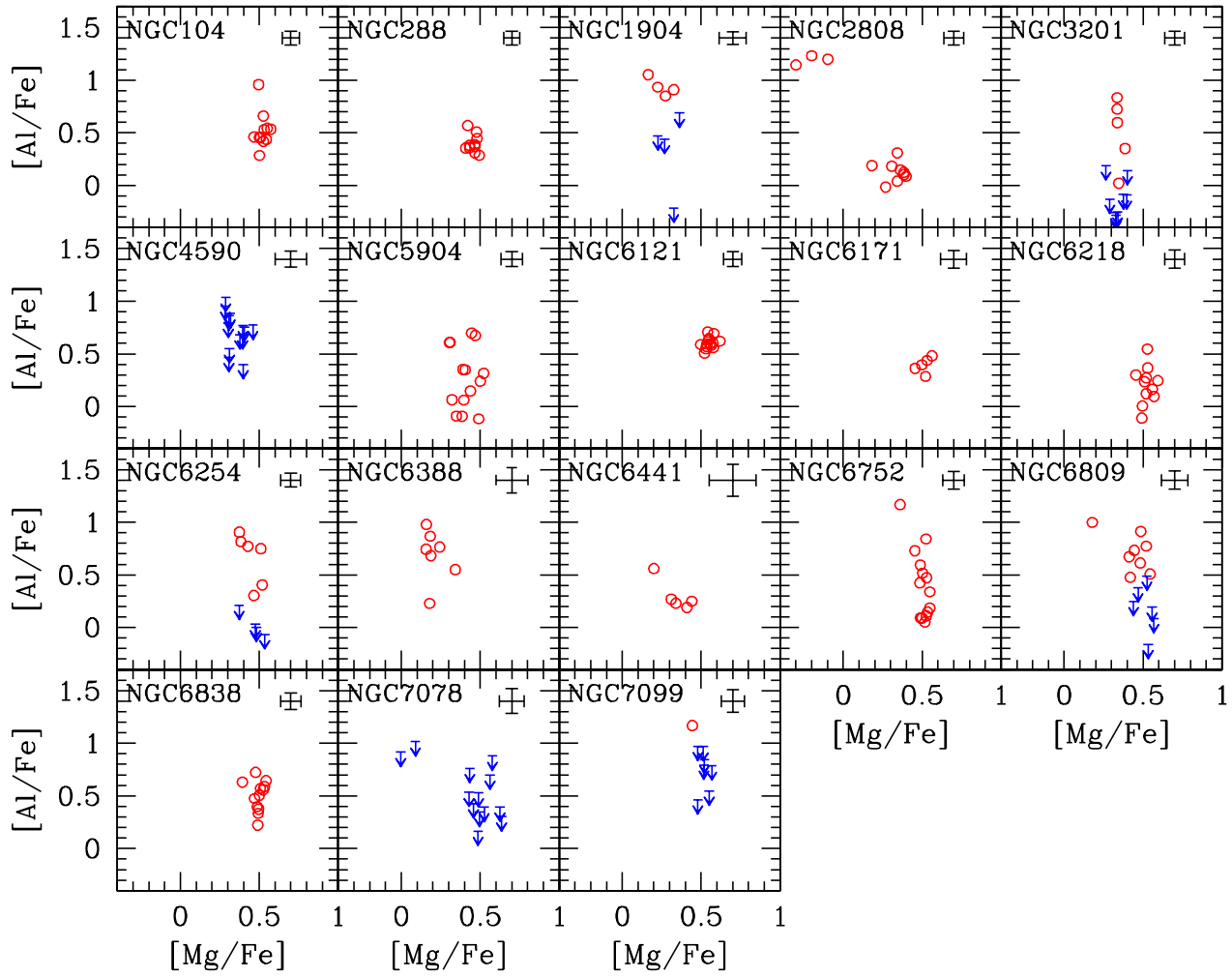

Fig. 6. The Mg-Al anticorrelation from UVES spectra observed in 18 of the 19 GCs of our project (including NGC 6388 from Paper VI and NGC 6441 from Paper III, but excluding NGC 6397, for which we did not measure Al). Star-to-star error bars (see Sect.4) are indicated in each panel. Upper limits are shown as arrows, detections as open circles.

lation between Si and Mg (elements for which we only have actual detections, no upper limits) to infer information on the *correlation* between Si and Al in individual GCs.

From data displayed in Fig. 7 we find that slopes statistically significant (at a level of at least 2σ) are found for NGC 2808, NGC 6388, NGC 6752, and NGC 7078. An enlargement for the Si-Mg anticorrelation in these clusters, together with the slopes and associated errors, is shown in the upper part of Fig. 10. In the bottom two panels of this figure we display the direct Si-Al correlations for the two clusters with significant slope and no upper limits on Al abundances: NGC 2808 and NGC 6752.

The explanation for this behaviour is given by Yong et al. (2005) in their study of giants in NGC 6752. The authors claim that such a correlation is expected if a "leakage" from the Mg-Al cycle on ^{28}Si does occur, and discuss how small amounts of ^{29}Si and ^{30}Si can even be synthesized by *neutron*−capture processes in the He-shell of AGB stars. However, the total abundance of Si is unlikely to change significantly unless the reaction ^{27}Al$(p,\gamma)^{28}$Si takes over the reaction ^{27}Al$(p,\alpha)^{24}$Mg in the Mg-Al chain. The result is that a certain amount of ^{28}Si might be produced in hot bottom burning (HBB) in intermediate-mass AGB stars by *proton*−capture reactions (see Karakas and Lattanzio 2003), giving just the sort of trend displayed in Fig. 10. Incidentally, the variation of Si abundances we found in NGC 6752 is exactly the same as that found by Yong et al. (2005).

A strong conclusion that can be drawn from the above results is that only a fraction of the polluters responsible for the Na-O anticorrelation actually produce large quantities of Al. This is likely to be related to the large difference between the temperature required for the two cycles. The temperature where the Mg-Al cycle occurs is high enough for a significant production of Si. As a result, the finding of the Si-Al correlation allows us to put a strong constraint on the temperature at which H-burning occurred in these massive clusters. By looking at the temperature dependence of Maxwellian-averaged reaction rates from NACRE for proton-captures (right panel of Fig. 8 in Arnould et al. 1999) we can evaluate that the reaction producing ^{28}Si becomes predominant in the Mg-Al cycle when the

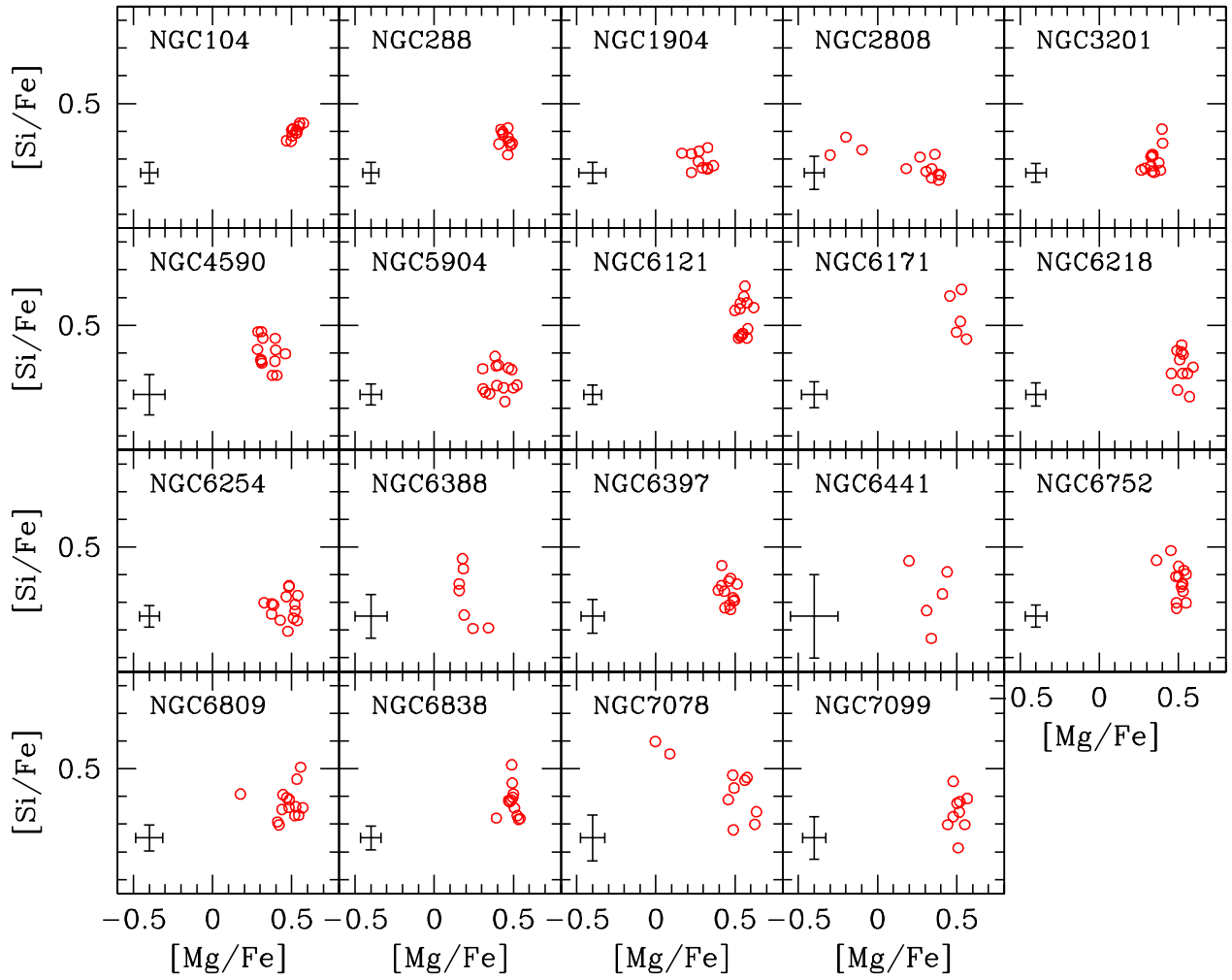

Fig. 7. The Mg-Si relation from UVES spectra of the 19 GCs of our project (including NGC 6388 from Paper VI and NGC 6441 from Paper III). Star-to-star error bars (see Sect.4) are indicated in each panel.

temperature exceeds $T_6 \sim 65$ K. Once again we then confirm that the chemical pattern we observe in present-day cluster red giants must already be imprinted in the gas by a previous generation of more massive stars. In currently evolving low-mass stars the CNO processing shell only reaches its maximum temperature of about 70 MK very near the tip of the RGB (e.g. Langer et al. 1996), while we observe stars still far from this magnitude range and yet able to show the Si-Al correlation in their photospheric abundances.

6. The Na-Al correlation: tuning a dilution model

New insights into the properties of the polluters can be obtained by relating the Mg-Al cycle with the Ne-Na cycle. A very fruitful approach is to compare the production of Na and Al.

We plotted in Fig. 11 the individual runs of Al and Na in each of the programme clusters. In most cases there is a clear correlation between Al and Na abundances. However, in spite of the numerous upper limits for metal-poor or Al-poor stars, it is also clear that these runs are different from cluster to cluster. In a few cases there is no appreciable change in the Al abundance, while Na abundances change by about 0.6 dex (see e.g. the case of NGC 6121=M 4), while in other clusters the Al abundances change much more than the Na ones. Thus, while

Table 11. Minimum and maximum abundances of Na and Al for the programme clusters from our dilution model

NGC	n	$[Na/Fe]_{min}$	$[Na/Fe]_{max}$	$[Al/Fe]_{min}$	$[Al/Fe]_{max}$	rms
104	11	0.15	0.74 ± 0.06	0.19 ± 0.11	0.72 ± 0.05	0.08
288	10	-0.10	0.71 ± 0.18	0.40 ± 0.02	0.50 ± 0.05	0.06
1904	8	-0.15	0.72 ± 0.07	−0.69 ± 0.24	0.91 ± 0.04	0.16
2808	12	-0.12	0.56 ± 0.04	−0.56 ± 0.17	1.03 ± 0.05	0.17
3201	13	-0.30	0.60 ± 0.09	−0.78 ± 0.24	0.60 ± 0.05	0.18
4590	12	-0.35	0.53 ± 0.13	< 0.15	< 0.65	
5904	14	-0.25	0.60 ± 0.10	−0.19 ± 0.08	0.61 ± 0.05	0.16
6121	14	-0.05	0.74 ± 0.08	0.59 ± 0.04	0.60 ± 0.09	0.05
6171	5	-0.05	0.69 ± 0.07	0.39 ± 0.10	0.40 ± 0.07	0.07
6218	11	-0.20	0.67 ± 0.07	0.07 ± 0.08	0.35 ± 0.08	0.12
6254	10	-0.30	0.56 ± 0.10	−0.84 ± 0.25	0.76 ± 0.04	0.28
6388	7	0.00	0.67 ± 0.05	−0.33 ± 0.80	0.78 ± 0.08	0.16
6397		-0.35	0.71 ± 0.23			
6441	5	-0.05	0.80 ± 0.10	−0.11 ± 0.23	0.51 ± 0.10	0.06
6752	14	-0.15	0.65 ± 0.07	−0.10 ± 0.09	0.73 ± 0.06	0.16
6809	14	-0.35	0.69 ± 0.09	−0.77 ± 0.39	0.83 ± 0.05	0.19
6838	12	0.00	0.76 ± 0.16	0.24 ± 0.13	0.73 ± 0.06	0.10
7078	13	< −0.05	0.70 ± 0.09	< 0.20	< 0.92	
7099	10	-0.20	0.76 ± 0.14	−0.55 ± 0.50	1.05 ± 0.14	0.07

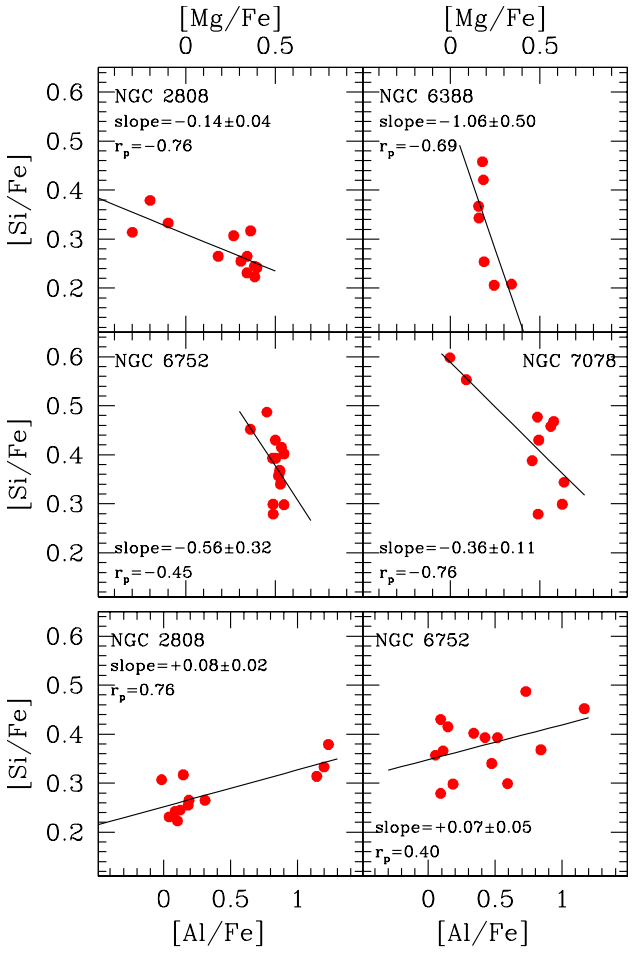

Fig. 10. Abundance ratios [Si/Fe] as a function of [Mg/Fe] in four GCs of our sample with significant slope of the Si-Mg anticorrelation (upper four panels). Abundance ratio [Si/Fe] as a function of [Al/Fe] for stars in NGC 2808 and NGC 6752 (bottom two panels).In each panel we report the slope and the linear regression coefficient of the correlation.

the Ne-Na and Mg-Al cycles are related, they do not occur in exactly the same polluting stars, and different clusters have different proportions of these different polluters.

To progress in our understanding of the relations between O depletion, the Ne-Na, and Mg-Al cycles, we make use of the dilution model considered in paper VII to explain the Na-O anticorrelation and how it changes from one cluster to another. A basic assumption of this model is that the polluting material has a well-defined composition, and the pattern of abundances in individual stars is simply obtained by diluting this polluting material with variable quantities of primordial material. As mentioned in Paper VII, this dilution model explains the shape of the Na-O anticorrelation (see also Prantzos et al. 2007). In this model the logarithmic abundance of an element [X] for a given dilution factor *dil* is given by

$$[X] = \log[(1 - dil)\ 10^{[\mathrm{Xo}]} + dil\ 10^{[\mathrm{Xp}]}], \quad (1)$$

where [Xo] and [Xp] are the logarithmic abundance of the element in the original and processed material, respectively. We apply this model to Na and Al abundances. We notice that a basic property of this model is that there should be a unique relation between Na and Al abundances in a given cluster. While this indeed seems the case for most of the clusters, there might be exceptions, the most notable being NGC 6254, for which there seems to be a genuine scatter of Al abundances at a given Na abundance. Let us ignore this difficulty for the moment. In principle, [Xo] and [Xp] could be directly derived from observations for both Na and Al. However, the sample of stars with UVES spectra is quite small for a single cluster, and it is very likely that the extremes of the distributions have not been well sampled. For Na, this concern can be removed by using the much larger samples of stars with GIRAFFE spectra: for Na we will adopt the values of [Xo]=$[\mathrm{Na/Fe}]_{\mathrm{min}}$ and [Xp]=$[\mathrm{Na/Fe}]_{\mathrm{max}}$ from Table 7 of Paper VII. On the other hand, we can only use the UVES data to derive $[\mathrm{Al/Fe}]_{\mathrm{min}}$ and $[\mathrm{Al/Fe}]_{\mathrm{max}}$. Since we could derive only upper limits for a number of stars, we applied a maximum likelihood method (see Isobe, Feigelson and Nelson 1986) to estimate $[\mathrm{Al/Fe}]_{\mathrm{min}}$ and $[\mathrm{Al/Fe}]_{\mathrm{max}}$ values, listed in Table 11.

Dilution sequences obtained by this approach are superimposed on the observed run of Na and Al abundances in Fig. 11. They generally do a good job of fitting the observations. However, there is a large scatter in the observational data for some clusters (e.g. NGC 6254). We think that there are a few cases where our dilution model is not fully compatible with observations, most likely because we cannot assume a single composition for the polluters.

In our model, $[\mathrm{Al/Fe}]_{\mathrm{min}}$ represents the original Al abundance in the cluster. We plotted the run of $[\mathrm{Al/Fe}]_{\mathrm{min}}$ with [Fe/H] in Fig. 12. We obtain low values of Al abundances in the most metal-poor clusters: in a couple of cases they are upper limits, because we did not detect Al lines in these clusters. Metal-rich clusters usually have very high values of $[\mathrm{Al/Fe}]_{\mathrm{min}}$. On the other hand, we find a huge range in Al abundances in clusters of intermediate metallicity. We will re-examine this point in a forthcoming paper, but only anticipate here that most of this scatter can be explained by the origin of these clusters (disc or inner halo versus outer halo clusters).

On the other hand, $[\mathrm{Al/Fe}]_{\mathrm{max}}$, or better the amount of Al produced[6], depends on the yields of typical polluters. It is then interesting to notice that we found $[\mathrm{Al/Fe}]_{\mathrm{prod}}$ to be correlated with a linear combination of metallicity and cluster luminosity, as shown in Fig. 13. This is true for all GCs in our sample except NGC 6838, which seems to have too large an Al production with respect to its metallicity and total mass. We have at present no explanation for this cluster so we excluded it from the fit. We note that this is the same combination of cluster metallicity and luminosity that we obtained from a multivariate analysis of $[\mathrm{O/Fe}]_{\mathrm{min}}$ in Paper VII (see Fig. 20 there). The implication is that the polluters that produced Al are actually the same as destroyed O and produced Na, but that their properties change regularly with cluster luminosity and metallicity.

The dependence on metallicity is not surprising, since HBB is expected to occur at a higher temperature in more metal-poor stars (see Lattanzio, Forestini and Charbonnel 2000). These stars can produce Al and destroy O more efficiently. On the

[6] $[\mathrm{Al/Fe}]_{\mathrm{prod}} = \log(10^{[\mathrm{Al/Fe}]_{\mathrm{max}}} - 10^{[\mathrm{Al/Fe}]_{\mathrm{min}}})$

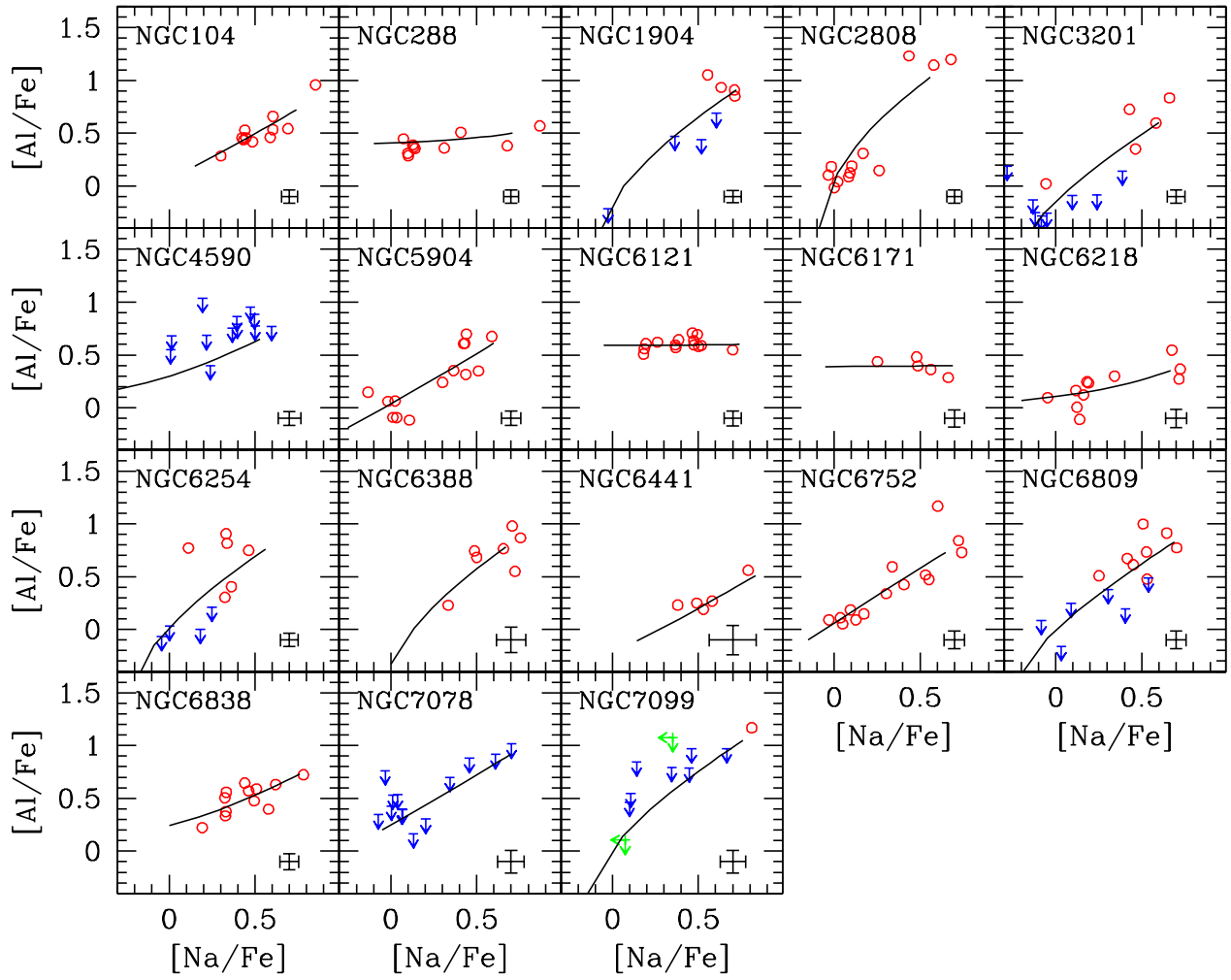

Fig. 11. [Al/Fe] ratios as a function of [Na/Fe] ratios for the 18 individual GCs, with a dilution model superimposed.

other hand, cluster luminosity is probably a proxy for the cluster mass, and the latter might be a proxy for polluter mass. This may be understood within the context that dynamical evolution of clusters occurs more rapidly in clusters of high mass (and luminosity). In this case, we should expect that the typical polluter mass is higher in more massive (and luminous) clusters. The trend towards increasing $[Al/Fe]_{max}$ and decreasing $[Na/Fe]_{max}$ and $[O/Fe]_{min}$ with increasing cluster luminosity should be a consequence of a similar trend with increasing typical polluter mass.

We may compare this result with the very recent nucleosynthetic yields for AGB polluters by Ventura & D'Antona. (2009). We indeed find similar trends over the mass range 4-6 $M_{\odot}$ (the mass range changes somewhat with metallicity, the value we give is for $Z = 10^{-3}$); however, the agreement is only qualitative. In the models Al production and O destruction are not enough, and/or Na production is much too sensitive to mass. As a consequence, even playing with the minimum and maximum mass of the polluters, we are never able to reproduce the abundances of all of these elements in any cluster. For instance, in the case of NGC 2808, we may obtain a reasonably good production of Na and Al; adopting a mass range for the polluters between 4.5 and 6.3 $M_{\odot}$ (and a Salpeter initial mass function -but this is not a critical assumption, given the narrow range of masses involved) we obtain [Na/Fe]~ 0.6 and [Al/Fe]~ 1.0, to be compared with $[Na/Fe]_{max}$=0.56 and $[Al/Fe]_{max}$=0.92. However, we get [O/Fe]~ −0.1, which is much larger than the observed value of $[O/Fe]_{min} = -1$ (see Paper VII). In the case of NGC 6121, a slightly wider mass range of the polluters (between 4.2 and 6.3 $M_{\odot}$) again reproduces the abundances of O and Na quite well ([O/Fe]~ 0 and [Na/Fe]~ 0.75, to be compared with $[O/Fe]_{min} = -0.2$ and $[Na/Fe]_{max}$=0.74), but it overestimates the production of Al ([Al/Fe]~ 1 against $[Al/Fe]_{max}$=0.65). We conclude that more improvement in the models is required for such a comparison to be meaningful.

We remind the reader that there are a few clusters for which a unique dilution sequence does not reproduce the run of [Al/Fe] with [Na/Fe]. Examples are NGC 3201, NGC 6254, and NGC 6809, but there are other more dubious cases, like NGC 5904. This result is not new, since Johnson et al. (2005) find a similar result for NGC 5272 (M 3). Such a result would suggest that in these clusters there were more generations of stars, or perhaps even a continuum of second generations. This

last hypothesis would agree better with the massive star polluters, where each polluter might have its own progeny.

Let us then consider the models for fast-rotating massive stars. We may use the yields given in Table 5 of Decressin et al. (2007), who give the predicted composition of the wind as a function of stellar mass. These models predict a roughly constant Na production and a production of Al and destruction of O that are an increasing function of the mass. This might indeed agree with observations. However, a closer look reveals several inconsistencies. First, Al production and O destruction change much less with mass than do the observed cluster to cluster variations in the maximum Al and minimum O abundances. This discrepancy becomes even worse if we consider that stars over quite wide mass ranges should be taken into account to provide enough mass for the second generation. A range in stellar rotation rates is no help, as it yields a range in Na abundances, which is not observed. This is the same difficulty as was found for the AGB model, and it may point toward basic problems in the relevant cross sections.

The rotating massive star scenario has an additional difficulty. In fact, in this scheme, material expelled from the polluting stars is not mixed into a single star-forming cloud, but rather second generation stars form around each of the fast-rotating, polluting massive stars. We then expect different O, Na, and Al yields, depending on the mass and rotation rate of the polluters. If we combine these different yields with a range in dilution factors, we expect that second-generation stars fill a triangle in the [Na/Fe] versus [Al/Fe] plane, the vertices being defined by the original [Na/Fe] and [Al/Fe] values, and by the [Na/Fe] and [Al/Fe] values given by the winds of the most and less massive fast-rotating star, respectively. The closer these last two values, the less is the mass range allowed for polluters. While a range in polluter masses seem indeed present in clusters like NGC 3201 or NGC 6254 (or NGC 5272=M 3: see Sneden et al. 2004), the sequences seem almost monoparametric in other clusters, including NGC 104 (47 Tuc), NGC 2808, NGC 6752 (see also Yong et al. 2003), or NGC 6205 (M 13, see Sneden et al. 2004). More extensive samples of stars with accurate determinations of the Al abundances are required to clarify this issue.

7. Summary

In this paper, we have derived atmospheric parameters, abundances of Fe and of the elements involved in proton capture at high temperatures (O, Na, Mg, Al, and Si) in 202 stars in 17 GCs. This analysis is based on FLAMES-UVES spectra. Adding the two clusters with similar data whose analysis has already been presented in previous papers (NGC 6441: Paper III; and NGC 6388: Paper VI), we now have a large data set (214 stars) from 19 GCs. This material complements results derived from the FLAMES-GIRAFFE spectra of about 2,000 stars, as discussed in Paper VII, providing abundance analysis for a sample of GC stars of unprecedented size.

The analysis of this huge dataset was done as automatically as possible. We put great care to reducing internal errors. Effective temperature were generally derived exploiting the $T_{\rm eff} - K$ magnitude relation within each cluster, calibrated using the relation between $T_{\rm eff}$ and $(V - K)$ colours. This allows us to minimise the impact of differential reddening (when present), and to reduce star-to-star errors in the effective temperatures to a few K. This was crucial for enabling us to discuss star-to-star abundance differences within each cluster.

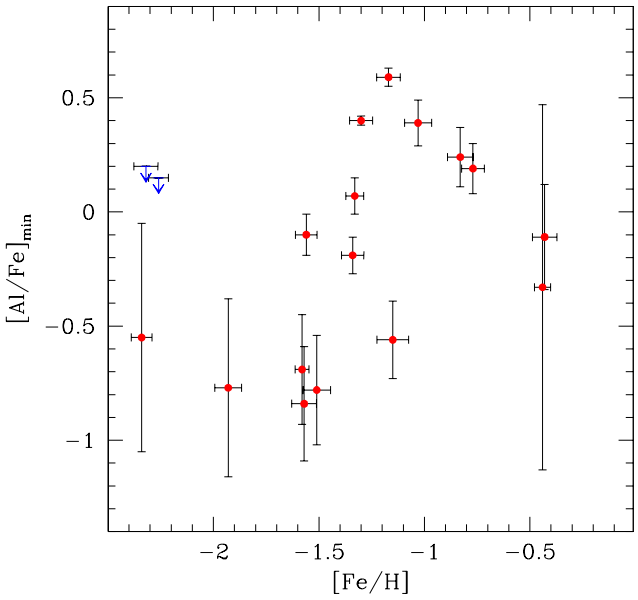

Fig. 12. $[Al/Fe]_{min}$ versus [Fe/H] for the 19 GCs; the two upper limits are for NGC 4590 and NGC 7078.

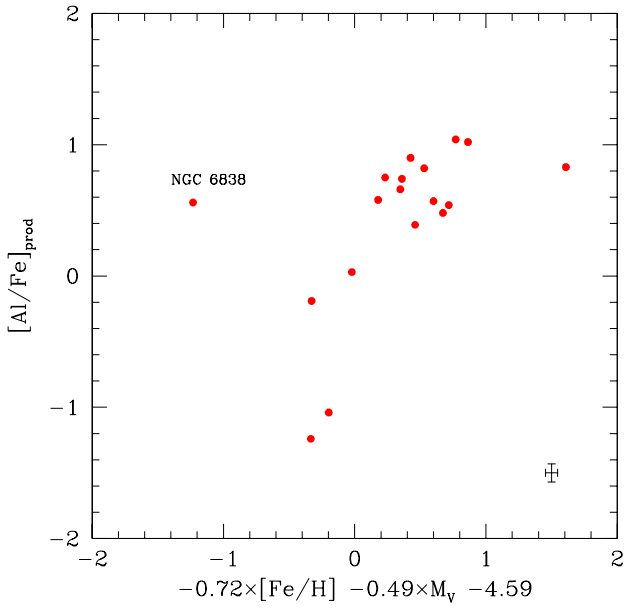

Fig. 13. Run of $[Al/Fe]_{prod}$ for the GC of our sample as a function of a linear combination of metallicity [Fe/H] and cluster luminosity M_V. The relation was computed excluding NGC 6838.

Data mining of this huge dataset is in progress. In the present paper, we focused on the star-to-star scatter in the abundances of O, Na, Mg, Al, and Si. This was very important for discussing the relation between the Ne-Na and Mg-Al cycles. The main results we obtained are as follows:

- We confirm the very small scatter in Fe abundances found in Paper VII. Regardless of the mechanism responsible for the variations in the abundances of O, Na, Mg, Al, and Si, it does not produce significant amounts of Fe.
- As in paper VII, we found variations in O and Na abundances (anticorrelated with each other) in all surveyed clusters, including small ones like NGC 288, NGC 6397, or NGC 6838 (M 71). While minimum O abundances change greatly from cluster to cluster, the maximum Na abundances show only a narrow spread. Clusters like NGC 288, NGC 6121 (M 4), and NGC 6171 (M 107) show no variation in the abundances of Al at all. This contrasts with the huge spread in the Al abundances found in other clusters, like NGC 2808, NGC 3201, NGC 6752. This clearly indicates that only a subset of the polluters responsible for the variations of the O and Na abundances are responsible for those of the Al abundances. That is, only a fraction of the polluting stars reached temperatures high enough for the Mg-Al cycle to be active.
- Significant variations in Mg and Si are seen whenever large overabundances of Al are observed. While the Mg depletion was expected in these cases, the observed overabundances of Si indicate that the "leakage" mechanism from the Mg-Al cycle proposed by Yong et al. (2005) to explain their data for NGC 6752, is in fact active also in other clusters. This requires temperatures above 65 MK for the Mg-Al cycle.
- We used a dilution model to derive minimum and maximum Al abundances from the Na-Al relation drawn from our UVES data, and minimum and maximum Na abundances obtained from the much more extensive GIRAFFE sample. These should reflect the primordial and polluter Al abundances, respectively. The peculiar run of the minimum Al abundances will be discussed in a forthcoming paper. However, from maximum and minimum Al abundances, we were able to derive the Al produced within the polluters. This was found to be correlated with the same combination of cluster luminosity (likely a proxy for the mass) and metallicity that we obtained from an examination of the minimum O abundances in Paper VII. This indicates that Al production and O destruction are closely related, possibly indicative of a common dependence on the typical mass of the polluters.
- A comparison of these results with current nucleosynthesis predictions from either massive AGB stars or fast-rotating massive stars shows that in both cases a qualitative, but not quantitative agreement can be obtained. Further theoretical work is clearly required.
- Finally, we found that our dilution model satisfactorily explains most of the clusters. However, the spread in Al abundances at a given Na abundance found in a few clusters (the clearer example being NGC 6254=M 10) shows that in some cases there was more than a single pool of gas from which second generation stars formed. We argue that a careful and extensive study of the Na-Al relation may provide crucial information on the nature of the polluters.

Acknowledgements. We wish to thank the ESO Service Mode personnel for their work, F. D'Antona for discussions, V. D'Orazi for her help, and the referee, Mike Bessell, for helping us to improve the paper. This publication makes use of data products from the Two Micron All Sky Survey, which is a joint project of the University of Massachusetts and the Infrared Processing and Analysis Center/California Institute of Technology, funded by the National Aeronautics and Space Administration and the National Science Foundation. This research has made use of the SIMBAD database, operated at CDS, Strasbourg, France and of NASA's Astrophysical Data System. This work was partially funded by the Italian MIUR under PRIN 2003029437. We also acknowledge partial support from the grant INAF 2005 "Experimenting nucleosynthesis in clean environments". SL is grateful to the DFG cluster of excellence "Origin and Structure of the Universe" for support.

References

Alonso, A., Arribas, S., Martinez-Roger, C. 1999, A&AS, 140, 261
Arnould, M., Goriely, S., Jorissen, A. 1999, A&A, 347, 572
Bekki, K. 2006, MNRAS, 367, L24
Bragaglia, A., Carretta, E., Gratton, R.G. et al. 2001, AJ, 121, 327
Carney, B.W. 1996, PASP, 108, 900
Carretta, E., Bragaglia, A., Gratton R.G., Leone, F., Recio-Blanco, A., Lucatello, S. 2006, A&A, 450, 523 (Paper I)
Carretta, E., Bragaglia, A., Gratton R.G., Lucatello, S., & Momany, Y. 2007a, A&A, 464, 927 (Paper II)
Carretta, E., Cohen, J. G., Gratton, R. G., Behr, B. B. 2001, AJ, 122, 1469
Carretta, E. et al. 2007b, A&A, 464, 967 (Paper VI)
Carretta, E. et al. 2007c, A&A, 464, 939 (Paper IV)
Carretta, E. et al. 2009, A&A, in press (Paper VII)
Cayrel, R. 1986, A&A, 168, 8
Charbonnel, C., Prantzos, N. 2006, in Globular Clusters, Guide to Galaxies, ed. T. Richtler, et al, Un. Concepcion (arXiv:astro-ph/0606220v1)
Cohen, J.G., Melendez, J. 2005, AJ, 129, 303
Cohen, J.G., Briley, M.M., Stetson, P.B. 2002, AJ, 123, 2525
Cohen, J. G., Gratton, R. G., Behr, B. B., Carretta, E. 1999, ApJ, 523, 739
Decressin, T., Meynet, G., Charbonnel C. Prantzos, N., Ekstrom, S. 2007, A&A, 464, 1029
Denisenkov, P.A., Denisenkova, S.N. 1989, A.Tsir., 1538, 11
Fulbright, J.P. 2000, AJ, 120, 1841
Fulbright,J.P., McWilliam, A., Rich M.R. 2007, ApJ, 661, 1152
Gehren, T., Shi, J.R., Zhang, H.W., Zhao, G., Korn, A.J. 2006, A&A, 451, 1065
Gratton, R.G., Bonifacio, P., Bragaglia, A., et al. 2001, A&A, 369, 87
Gratton, R.G., Carretta, E., Claudi, R., Lucatello, S., Barbieri, M. 2003, A&A, 404, 187
Gratton, R.G., Carretta, E., Eriksson, K., Gustafsson, B. 1999, A&A, 350, 955
Gratton, R.G., Lucatello, S., Bragaglia, A., Carretta, E., Momany, Y., Pancino, E., Valenti, E. 2006, A&A, 455, 271 (Paper III)
Gratton, R.G., Sneden, C., & Carretta, E. 2004, ARA&A, 42, 385
Gratton, R.G., Sneden, C., Carretta, E., & Bragaglia, A. 2000, A&A, 354, 169
Gratton, R.G. et al. 2007, A&A, 464, 953 (Paper V)

Harris, W. E. 1996, AJ, 112, 1487
Isobe, T., Feigelson, E.D., Nelson, P.I. 1986, ApJ, 306, 490
Ivans, I. I., Kraft, R. P., Sneden, C., Smith, G. H., Rich, R. M., Shetrone, M. 2001, AJ, 122, 1438
Ivans, I. I., Sneden, C., Kraft, R. P., Suntzeff, N. B., Smith, V. V., Langer, G. E., Fulbright, J. P. 1999, AJ, 118, 1273
Johnson, C.I., Kraft, R.P., Pilachowski, C.A., Sneden, C., Ivans, I.I., Benman, G. 2005, PASP, 117, 1308
Johnson, J. 2002, ApJS, 139, 219
Jonsell, K., Edvardsson, B., Gustaffsson, B., Magain, P., Nissen, P.E., Asplund, M. 2005, A&A, 440, 321
Karakas, A., Lattanzio, J.C. 2003, PASA, 20, 279
Kraft, R.P. 1994, PASP, 106, 553
Kurucz, R.L. 1993, CD-ROM 13, Smithsonian Astrophysical
Langer, G.E., Hoffman, R., & Sneden, C. 1993, PASP, 105, 301
Langer, G.E., Hoffman, R., Zaidins, C.S.. 1996, PASP, 109, 244
Lattanzio, J.C., Forestini, M., Charbonnel, C. 2000, MemSAIt, 71, 737
Mackey, A.D., van den Bergh, S. 2005, MNRAS, 360, 631
Magain, P. 1984, A&A, 134, 189
Parmentier, G., Gilmore, G. 2001, A&A, 378, 97
Pasquini, L., et al. 2002, The Messenger, 110, 1
Piotto et al. 2005, ApJ, 621, 777
Piotto et al. 2007, ApJ, 661, L53
Prantzos, N., Charbonnel, C., 2006, A&A, 458, 135
Prantzos, N., Charbonnel, C., Iliadis, C. 2007, A&A, 470, 179
Reddy, B.E., Tomkin, J., Lambert, D.L., Allende prieto, C. 2003, MNRAS, 340, 304
Skrutskie, M.F., et al. 2006, AJ, 131, 1163
Sneden, C., Kraft, R.P., Guhathakurta, P., Peterson, R.C., Fulbright, J.P. 2004, AJ, 127, 2162
Venn, K.A., Irwin, M., Shetrone, M.D., Tout, C.A., Hill, V., Tolstoy, E. 2004, AJ, 128, 1177
Ventura, P., D'Antona, F. 2009, A&A, 499, 835
Ventura, P., D'Antona, F., Mazzitelli, I., Gratton, R. 2001, ApJ, 550, L65
Yong, D., Grundahl, F., Lambert, D.L., Nissen, P.E., Shetrone, M.D. 2003, A&A,402, 985
Yong, D., Grundahl, F., Nissen, P.E., Jensen, H.R., Lambert, D.L. 2005, A&A, 438, 875